

Dalton Transactions

Accepted Manuscript



This is an *Accepted Manuscript*, which has been through the Royal Society of Chemistry peer review process and has been accepted for publication.

Accepted Manuscripts are published online shortly after acceptance, before technical editing, formatting and proof reading. Using this free service, authors can make their results available to the community, in citable form, before we publish the edited article. We will replace this *Accepted Manuscript* with the edited and formatted *Advance Article* as soon as it is available.

You can find more information about *Accepted Manuscripts* in the [Information for Authors](#).

Please note that technical editing may introduce minor changes to the text and/or graphics, which may alter content. The journal's standard [Terms & Conditions](#) and the [Ethical guidelines](#) still apply. In no event shall the Royal Society of Chemistry be held responsible for any errors or omissions in this *Accepted Manuscript* or any consequences arising from the use of any information it contains.

Mixed-ligand hydroxocopper(II)/pyridazine clusters embedded into 3D framework lattices†

Anna S. Degtyarenko,^a Marcel Handke,^b Karl W. Krämer,^c Shi-Xia Liu,^{*c} Silvio Decurtins,^c Eduard B. Rusanov,^d Laurence K. Thompson,^e Harald Krautscheid^b and Konstantin V. Domasevitch^{*a}

5 *Receipt/Acceptance Data* [DO NOT ALTER/DELETE THIS TEXT]

Publication data [DO NOT ALTER/DELETE THIS TEXT]

DOI: 10.1039/b000000x [DO NOT ALTER/DELETE THIS TEXT]

Rational combination of pyridazine, hydroxo and carboxylate bridging ligands led to the assembly of three types of mixed-ligand polynuclear Cu(II) clusters (**A**: [Cu₂(μ-OH)(μ-pdz)(μ-COO)]; **B**:
 10 [Cu₄(μ₃-OH)₂(μ-pdz)₂]; **C**: [Cu₅(μ-OH)₂(μ-pdz)₄(μ-COO)₂(μ-H₂O)₂]) and their integration into 3D framework structures. Mixed-ligand complexes [Cu₂(μ-OH){TMA}(L)(H₂O)] (**1**), [Cu₄(μ₃-OH)₂{ATC}(L)₂(H₂O)]·H₂O (**2**) [Cu₄(μ₃-OH)₂{TDC}(L)₂(H₂O)]·7H₂O (**3**) (L = 1,3-bis(pyridazin-4-yl)adamantane; TMA³⁻ = benzene-1,3,5-tricarboxylate, ATC³⁻ = adamantane-1,3,5-tricarboxylate, TDC²⁻ = 2,5-thiophenedicarboxylate) and [Cu₅(μ-OH)₂{X}₄(L)₂(H₂O)₂]·nH₂O (X =
 15 benzene-1,3-dicarboxylate, BDC²⁻, n = 5 (**4**) and 5-hydroxybenzene-1,3-dicarboxylate, HO-BDC²⁻, n = 6 (**5**)) are prepared under hydrothermal conditions. Trigonal bridges TMA³⁻ and ATC³⁻ generate planar Cu(II)/carboxylate subtopologies further pillared into 3D frameworks (**1**: binodal 3,5-coordinated, doubly interpenetrated **tcj**-3,5-Ccc2; **2**: binodal 3,8-coordinated **tfz**-d) by bitopic pyridazine ligands. Unprecedented triple bridges in **1** (cluster of type **A**) support short Cu...Cu
 20 separations of 3.0746(6) Å. The framework in **3** is a primitive cubic net (**pcu**) with multiple *bis*-pyridazine and TDC²⁻ links between the tetranuclear nodes of type **B**. Compounds **4** and **5** adopt uninodal ten-coordinated framework topologies (**bct**) embedding unprecedented centrosymmetric open-chain pentanuclear clusters of type **C** with two kinds of bridges, Cu(μ-OH)(μ-pdz)₂Cu and Cu(μ-COO)(μ-H₂O)Cu (Cu...Cu distances are 3.175 and 3.324 Å, respectively).
 25 Magnetic coupling phenomena were detected for every type of cluster by susceptibility measurements of **1**, **3** and **4**. For binuclear clusters **A** in **1**, the intracuster antiferromagnetic exchange interactions lead to a diamagnetic ground state (*J* = -17.5 cm⁻¹; *g* = 2.1). Strong antiferromagnetic coupling is relevant also for the type **B**, which consequently results in a diamagnetic ground state (*J*₁ = -110 cm⁻¹; *J*₂ = -228 cm⁻¹, *g* = 2.07). For pentanuclear clusters of
 30 type **C** in **4**, the exchange model is based on a strongly antiferromagnetically coupled central linear trinuclear Cu₃ group (*J*₁ = -125 cm⁻¹) and two outer Cu centers weakly antiferromagnetically coupled to the terminal Cu ions of the triad (*J*₂ = -12.5 cm⁻¹).

Introduction

The study of metal-organic framework (MOF) structures
 35 adopted by linkage of polynuclear metal ion clusters is a special topic of coordination and materials chemistry and crystal engineering, which attracts a rapidly growing interest during the last decade.¹ In view of framework topologies,² the

design of such solids presents a particularly successful
 40 approach. It allows to avoid common limitations for the node connections imposed by the typical coordination numbers,³ and therefore a diversity of extremely highly-connected frameworks became accessible by propagation of coordination geometries established by polynuclear clusters.⁴ Even a more
 45 important aspect considers the utility of the latter for functionalization of the MOFs towards specific applications in magnetism and catalysis,⁵ while imprinting the inherent properties of the clusters into the extended lattices.⁶ Therefore, the developing of polynucleating ligand systems,
 50 which combine abilities for generation of polynuclear fragments⁷ and their further integration into the framework, receives a special value.⁸

^a *Inorganic Chemistry Department, Taras Shevchenko National University of Kyiv, Volodymirska Street 64/13, Kyiv 01601, Ukraine*
E-mail: dk@univ.kiev.ua (K.V.D.)

^b *Institut für Anorganische Chemie, Universität Leipzig, Johannisallee 29, D-04103 Leipzig, Deutschland*

^c *Departement für Chemie und Biochemie, Universität Bern, Freiestrasse 3, CH-3012 Bern, Switzerland*
E-mail: liu@iac.unibe.ch (S.-X.L.)

^d *Institute of Organic Chemistry, Murmanskaya Str. 4, Kyiv 253660, Ukraine.*

^e *Department of Chemistry, Memorial University of Newfoundland, St. John's, A1B 3X7, Canada*

† Electronic Supplementary Information (ESI) available: Details for organic synthesis and characterization; IR spectra, TGA and thermo-XRPD patterns; X-ray structure refinement. See <http://dx.doi.org/10.1039/b000000x/>

Table 1 Bridging coordination of non-chelating pyridazines towards Cu(II) ions^a

Complex	co-Bridge(s)	Cu...Cu/ Å	Structural pattern and magnetic features	Ref.
[Cu(OH)(sac)(μ-pdz)] _n	μ-OH, μ-sac- <i>N,O</i>	3.360	1D chain of triply bridged Cu ²⁺ ions; strong AFM, μ _{eff} (RT) = 0.99 μ _B	22
[Cu(μ-pdz)Cl ₂] _n	μ-Cl (×2)	3.378	1D chain of triply bridged Cu ²⁺ ions; μ _{eff} (RT) = 1.5-1.7 μ _B ; low-temperature AF coupling	20a, 23
[Cu(OH)(μ-pdz)(NO ₃) ₂] _n	μ-OH, μ-NO ₃ - <i>O,O'</i>	3.322	1D chain of triply bridged Cu ²⁺ ions; strong AFM, μ _{eff} (RT) = 1.08 μ _B	19
[Cu ₃ (μ-pdz) ₄ (pdz) ₂ (μ-NO ₃) ₂ (NO ₃) ₄]	μ-NO ₃ - <i>O,O</i>	3.406	Triple bridges [M(μ-pdz) ₂ (μ-NO ₃)M]; Discrete trinuclear; strong AFM, μ _{eff} (RT) = 1.51 μ _B	15, 19
[Cu ₃ (OH) ₂ (μ-bpdz) ₃ (H ₂ O) ₂ {CF ₃ CO ₂] ₂] ²⁺	μ-OH	3.236	Discrete trinuclear, triple bridges [M(μ-pdz) ₂ (μ-OH)M]	13
[Cu(OH)(pp)(H ₂ NSO ₃)·H ₂ O]	μ-OH	3.394	1D chain of triply bridged Cu ²⁺ ions	14a
[Cu ₂ (OH){TMA}(L)(H ₂ O)]	μ-OH, μ-RCO ₂ - <i>O,O'</i>	3.075	Discrete binuclear cluster with triply bridged Cu ²⁺ ions	This work
[Cu ₄ (OH) ₂ {ATC} ₂ (L) ₂ (H ₂ O) ₂ ·H ₂ O]	μ ₃ -OH	3.272	Discrete tetranuclear cluster	This work
[Cu ₄ (OH) ₂ {TDC} ₃ (L) ₂ (H ₂ O) ₂ ·7H ₂ O]	μ ₃ -OH	3.334	The same	This work
[Cu ₅ (OH) ₂ {BDC} ₄ (L) ₂ (H ₂ O) ₂ ·5H ₂ O]	μ-OH	3.175	Discrete pentanuclear cluster with a trinuclear triply-bridged skeleton M{(μ-pdz) ₂ (μ-OH)M} ₂	This work
[Cu ₅ (OH) ₂ {HO-BDC} ₄ (L) ₂ (H ₂ O) ₂ ·6H ₂ O]	μ-OH	3.187	The same	This work

^a sac = saccharinate; bpdz = 4,4'-bipyridazine; pp = pyridazino[4,5-*d*]pyridazine; L = 1,3-*bis*(pyridazin-4-yl)adamantane; BDC = isophthalate; HO-BDC = 5-hydroxyisophthalate; TDC = thiophene-2,5-dicarboxylate; TMA = benzene-1,3,5-tricarboxylate; ATC = adamantane-1,3,5-tricarboxylate.

60 with corresponding phthalazine, 1,2,4-triazole, 1,2,4-triazolate and pyrazolate analogs.⁹ The ability of pyridazine to generate polynuclear complexes with tunable spin states of the metal ions is also known.¹⁰ The attractiveness of polypyridazinyl ligands, however, was limited until now because of their low chemical accessibility. Actually, the preparative chemistry involving pyridazine relies on only one general method which is applicable for facile functionalization of different substrates, namely on a very simple click reaction¹¹ involving inverse electron demand cycloadditions of 1,2,4,5-tetrazine.¹² Recent developments make this key intermediate readily available^{12,13} thus offering flexible pathways towards pyridazine ligands.^{13,14} A second potential drawback one might find in the inherent coordination ability of pyridazine.^{13,14} It manifests a pronounced affinity towards d¹⁰ Cu(I) and Ag(I) ions, commonly generating either single, double or triple bridges between the metallic centres involved in the desired and peculiar polynuclear and polymeric motifs.^{14,17} In the case of divalent *d*-metal ions, bridging coordination of this electron deficient and low basic ligand (p*K*_a = 2.24 for pyridazine vs. p*K*_a = 5.25 for pyridine) is less characteristic and predictable, compared with a simple monodentate pyridine-like function.^{15,18} Nevertheless, double coordination of pyridazine may be stabilized under utilization of suitable complementary short-distance co-bridges, such as hydroxo,^{10,13,19} halogenido,²⁰ nitrate,¹⁵ isothiocyanato,^{10,21} saccharinato,²² and actually every of the reports for pyridazine bridges between 3d-metal ions considers such a multiple heteroligand linkage, which is best illustrated by a Cu(II) series (Table 1). Thus a promising approach towards development of nanosized molecular magnets may rely on a synergism of the ligands in multicomponent systems²⁴ based upon bifunctional pyridazines, which could be well suited for the synthesis of extended frameworks incorporating polynuclear cluster units.

95 In this work we report the construction of unprecedented discrete di-, tetra- and pentanuclear copper(II)/pyridazine clusters and their integration into the 3D MOFs structures by a

concerted action of representative di- and tricarboxylate linkers (H₂BDC = isophthalic acid; H₂HO-BDC = 5-hydroxyisophthalic acid; H₂TDC = thiophene-2,5-dicarboxylic acid; H₃TMA = trimesic acid; H₃ATC = adamantane-1,3,5-tricarboxylic acid) and prototypical pyridazine tecton 1,3-*bis*(pyridazin-4-yl)adamantane (L) (Scheme 1), which features a doubled ligand functionality established at a rigid alicyclic molecular platform.

Results and Discussion

Structure of the coordination compounds

All the compounds adopt 3D framework structures based upon multinuclear heteroligand clusters, which represent topological net nodes and thus provide a primary factor for the complicated connectivities. Three types of the observed clusters, such as binuclear in **1**, tetranuclear in **2**, **3** and pentanuclear units in **4** and **5** (Scheme 2), originate in a combination of three kinds of ligand bridges (pyridazine, hydroxo and carboxylate), while preserving a common simple submotif in the form of Cu ions linked by a double pdz/OH bridge. This suggests a perfect compatibility of μ-pdz and μ-OH linkers, which are commonly concomitant and act in a synergetic manner.^{10,13,19} In fact, the significance of the hydroxo bridges is most crucial for the present systems since the bidentate coordination of pyridazine itself is less applicable for the chemistry of transition metal dications, as stated above. In this view, the clusters demonstrate a clear structural hierarchy, which implies a basic hydroxocopper(II) core, pyridazine co-bridges, auxiliary carboxylate ligands and additional monodentate pyridazine and aqua donors. The function of the carboxylate is most important for the compounds **4** and **5**, providing expansion of the trinuclear [Cu₃(μ-pdz)₄(μ-OH)₂] skeleton to a pentanuclear architecture. Especially close structural relationship may be found for binuclear (**A**) and tetranuclear (**B**) motifs. Doubling the cluster nuclearity is made possible by elimination of the carboxylate bridge and a simple dimerization along the Cu-

Table 2 Highly-connected topologies of MOFs 1-5

Complex	Cluster type	Ligand coordination	Dimensionality	Net nodes (coordination)	Schläfli symbol	Topological type
1	A	3	2D → 3D ^a	[Cu ₂ (μ-OH)] (5), TMA (3)	{6 ³ }{6 ⁹ .8}	tcj -3,5-Ccc2
2	B	3	2D → 3D ^a	[Cu ₄ (μ ₃ -OH) ₂] (8), ATC (3)	{4 ³ } ₂ {4 ⁶ .6 ¹⁸ .8 ⁴ }	tfz -d (UO ₃)
3	B	3	3D	[Cu ₄ (μ ₃ -OH) ₂] (6)	{4 ¹² .6 ³ }	pcu (α-Po)
4	C	4	3D	[Cu ₅ (μ-OH) ₂] (10)	{3 ¹² .4 ²⁸ .5 ⁵ }	bct
5	C	4	3D	[Cu ₅ (μ-OH) ₂] (10)	{3 ¹² .4 ²⁸ .5 ⁵ }	bct

^a Dimensionality of the Cu/carboxylate subtopology and the overall dimensionality of the resulting heteroligand frameworks.

Table 3 Selected bond distances (Å) and angles (°) for [Cu₂(μ-OH){TMA}(L)(H₂O)] (1)^a

Cu1-O3	2.0418(18)	O3-Cu1-N1	89.10(8)
Cu1-N4 ⁱ	2.043(2)	O3-Cu1-O7 ⁱⁱ	115.76(8)
Cu1-N1	2.053(2)	N4 ⁱ -Cu1-O7 ⁱⁱ	89.91(9)
Cu1-O7 ⁱⁱ	2.1577(16)	N1-Cu1-O7 ⁱⁱ	84.24(7)
		O3-Cu1-N4 ⁱ	91.75(9)
		N4 ⁱ -Cu1-N1	173.85(9)
Disordered fragment			
<i>Orientation A</i>		<i>Orientation B</i>	
Cu1-O1A	1.873(3)	Cu1-O1B	1.913(3)
Cu2A-O1A	1.906(3)	Cu2B-O1B	1.895(4)
Cu2A-O5 ⁱⁱⁱ	1.946(2)	Cu2B-O6 ⁱⁱⁱ	1.9264(19)
Cu2A-O4	1.984(2)	Cu2B-O8 ⁱⁱ	1.9307(18)
Cu2A-O2A	1.991(3)	Cu2B-O2B	1.952(4)
Cu2A-N2A	2.207(4)	Cu2B-N2B	2.262(4)
O1A-Cu1-N4 ⁱ	91.62(12)	O1B-Cu1-N4 ⁱ	86.79(12)
O1A-Cu1-N1	93.80(12)	O1B-Cu1-N1	96.27(12)
O1A-Cu2A-O5 ⁱⁱⁱ	87.56(13)	O1B-Cu2B-O6 ⁱⁱⁱ	88.57(13)
O1A-Cu2A-O4	88.78(14)	O1B-Cu2B-O8 ⁱⁱ	91.98(12)
O5 ⁱⁱⁱ -Cu2A-O4	155.29(11)	O6 ⁱⁱⁱ -Cu2B-O8 ⁱⁱ	159.17(9)
O1A-Cu2A-O2A	178.92(17)	O1B-Cu2B-O2B	178.52(14)
O1A-Cu2A-N2A	88.73(14)	O1B-Cu2B-N2B	87.98(15)
O5 ⁱⁱⁱ -Cu2A-N2A	109.02(13)	O6 ⁱⁱⁱ -Cu2B-N2B	104.15(12)
O4-Cu2A-N2A	95.32(13)	O8 ⁱⁱ -Cu2B-N2B	96.68(12)
Cu2A-O1A-Cu1	108.89(16)	Cu2B-O1B-Cu1	110.43(16)

^a Symmetry codes: (i) -0.5+x, -0.5+y, z; (ii) x, -y, 0.5+z; (iii) x, 1-y, 0.5+z.

OH sides with formation of two edge-sharing [Cu₃(μ₃-OH)]
135 fragments. Such a “dimer”, often encountered for different combinations of bridging ligands, is particularly characteristic for the hydroxocopper systems.²⁵ Further intercluster connection with generation of frameworks occurs by an interplay of bipyridazine (as bitopic linker between the
140 clusters, establishing three or four Cu-N bonds) and dicarboxylate bridges (TDC²⁻ (**3**), BDC²⁻ (**4**), HO-BDC²⁻ (**5**)), which are equally important in the view of the resulting topologies. This is contrary to the tricarboxylate (TMA³⁻ (**1**), ATC³⁻ (**2**)) frameworks. Trifunctional anions, as the three-
145 coordinated nodes, provide an additional origin of connectivity and generate distinct planar Cu-carboxylate subtopologies, further pillared with bitopic bipyridazine ligands (Table 2).

A simpler binuclear cluster **A** was observed in [Cu₂(μ-OH){TMA}(L)(H₂O)] (**1**), with an unprecedented mixed-ligand pdz/OH/carboxylate triple bridge connecting two Cu ions at very short distances of Cu1...Cu2A 3.0746(6) Å and Cu1...Cu2B 3.1270(7) Å (for two orientations of the disordered fragment). The environments of metal ions are
155 completed with monodentate carboxylate and pyridazine groups and aqua ligands (Figure 1, Table 3). As it was

indicated by the values of Addison τ parameters,²⁶ the geometries of the coordination polyhedra are intermediate between idealized trigonal-bipyramidal (τ = 1) and square-pyramidal (τ = 0) extremes: for the orientation A, τ = 0.66 (Cu1) and 0.39 (Cu2A); for the orientation B, Cu1, τ = 0.53 (Cu1) and 0.32 (Cu2B).

The low nuclearity of the cluster is likely a consequence of topology limitations imposed by the rigid trigonal triple-charged TMA³⁻ connector: the planar Cu/carboxylate subtopology in the form of a hexagonal net (Figure 1b), clearly implies a three-fold coordination of the hydroxocopper nodes and their complementary charge of 3+ [e.g. Cu₂(μ-OH)]. The bipyridazine ligands are accommodated at both
170 axial sides of this plane, and they connect pairs of the clusters at a distance of 13.56 Å and expand the structure in a third dimension as pillars between the successive hexagonal layers. The result is a rare binodal three- and five-connected {6³}{6⁹.8} net (three-letter notation is **tcj**-3,5-Ccc2), which
175 appears to be very open and therefore, two identical nets interpenetrate (Figure 2). That is a class IIa interpenetration, Z = 2, with a full symmetry element $\bar{1}$.^{27,28}

A comparable morphology of the framework is observed for the aliphatic analog of trimesic acid, 1,3,5-adamantanetricarboxylate (ATC³⁻) in [Cu₄(μ₃-OH)₂{ATC}(L)₂(H₂O)₂·H₂O (**2**). That is a first coordination polymer generated by this ligand and we introduce ATC³⁻ as a novel geometrically rigid tripodal linker, potentially complementing and expanding the chemistry of functional
185 frameworks based upon TMA³⁻ (such as HKUST-1).²⁹ Both metal ions adopt typical Jahn-Teller polyhedra in the form of square pyramids (Cu1; Addison parameter²⁶ τ = 0.18) or axially elongated octahedra (Cu2) (Table 4), with pyridazine-N donors positioned at the equatorial planes. In the metal-carboxylate subtopology, the net nodes exist as the above six-connected tetranuclear clusters [Cu₄(μ₃-OH)₂] and three-connected ATC³⁻ (in 1:2 proportions), giving rise to a 2D structure of the CdI₂ or Mg(OH)₂ type (Kagomé dual net, {4³}₂{4⁶.6⁶.8³}), three-letter notation “**kgd**”) (Figure 3). Pairs
195 of the bipyridazine ligands, as double links, interconnect the clusters from the successive layers (separated at 12.83 Å), yielding a 3D eight- and three-coordinated framework, with a Schläfli point symbol {4³}₂{4⁶.6¹⁸.8⁴} (**tfz**-d, topological type of UO₃) (Table 2). There is a limited number of structural precedents for such a linkage, most of which also incorporate
200 polynuclear cluster nodes and trigonal TMA³⁻ links.³⁰

Similar tetranuclear net nodes are also observed for [Cu₄(μ₃-OH)₂{TDC}(L)₂(H₂O)₂·7H₂O (**3**). However, substitution of the carboxylate portion of the structure for

Table 4 Selected bond distances (Å) and angles (°) for tetranuclear complexes **2** and **3**^a

[Cu ₄ (μ ₃ -OH) ₂ {ATC} ₂ (L) ₂ (H ₂ O) ₂ ·H ₂ O (2)			
Cu1-O1	1.931(2)	Cu2-O6 ⁱⁱ	1.948(3)
Cu1-O2	1.952(3)	Cu2-O5 ⁱⁱⁱ	1.953(3)
Cu1-N4 ^{iv}	2.026(3)	Cu2-O1	1.962(2)
Cu1-N1	2.068(3)	Cu2-N2	2.016(3)
Cu1-O1w	2.359(3)	Cu2-O1 ⁱ	2.423(2)
O1-Cu1-O2	167.55(11)	O6 ⁱⁱ -Cu2-O5 ⁱⁱⁱ	85.36(12)
O1-Cu1-N4 ^{iv}	94.38(12)	O6 ⁱⁱ -Cu2-O1	97.84(11)
O2-Cu1-N4 ^{iv}	93.50(12)	O5 ⁱⁱⁱ -Cu2-O1	176.64(12)
O1-Cu1-N1	86.13(12)	O6 ⁱⁱ -Cu2-N2	173.27(12)
O2-Cu1-N1	86.29(12)	O5 ⁱⁱⁱ -Cu2-N2	90.36(12)
N4 ^{iv} -Cu1-N1	178.20(13)	O1-Cu2-N2	86.36(12)
O1-Cu1-O1w	100.77(10)	O6 ⁱⁱ -Cu2-O1 ⁱ	99.00(10)
N4 ^{iv} -Cu1-O1w	90.72(12)	O1-Cu2-O1 ⁱ	85.52(10)
N1-Cu1-O1w	87.49(11)	N2-Cu2-O1 ⁱ	86.53(11)
Cu1-O1-Cu2	114.38(12)	Cu2-O1-Cu2 ⁱ	94.48(10)
Cu1-O1-Cu2 ⁱ	120.24(12)		
[Cu ₄ (μ ₃ -OH) ₂ {TDC} ₃ (L) ₂ (H ₂ O) ₂ ·7H ₂ O (3)			
Cu1-O1	1.920(2)	Cu2-O1	1.919(2)
Cu1-O1 ⁱ	2.352(2)	Cu2-O6	1.968(2)
Cu1-O2	1.942(11)	Cu2-N4 ⁱⁱⁱ	2.007(3)
Cu1-O8 ⁱⁱ	1.952(2)	Cu2-N2	2.058(3)
Cu1-O5 ^{iv}	1.959(12)	Cu2-O10	2.236(2)
Cu1-N1	2.052(3)		
O1-Cu1-O2	160.6(3)	O1-Cu2-O6	172.67(10)
O1-Cu1-O8 ⁱⁱ	97.53(10)	O1-Cu2-N4 ⁱⁱⁱ	91.96(10)
O2-Cu1-O8 ⁱⁱ	84.5(4)	O6-Cu2-N4 ⁱⁱⁱ	87.77(11)
O1-Cu1-N1	88.00(10)	O1-Cu2-N2	88.41(10)
O2-Cu1-N1	90.8(4)	O6-Cu2-N2	89.29(10)
O8 ⁱⁱ -Cu1-N1	174.25(11)	N4 ⁱⁱⁱ -Cu2-N2	159.51(12)
O5 ^{iv} -Cu1-N1	83.1(3)	O1-Cu2-O10	93.71(9)
O1-Cu1-O1 ⁱ	85.37(9)	O6-Cu2-O10	93.25(10)
N1-Cu1-O1 ⁱ	94.72(10)	N2-Cu2-O10	90.06(10)
Cu1-O1-Cu1 ⁱ	94.63(9)	Cu2-O1-Cu1 ⁱ	110.79(10)
Cu2-O1-Cu1	120.57(12)		

^a Symmetry codes for **2**: (i) $-x, 2-y, 1-z$; (ii) $-1+x, y, z$; (iii) $1-x, 1-y, 1-z$; (iv) $x, y, -1+z$. For **3**: (i) $1-x, 2-y, -z$; (ii) $-0.5+x, 2.5-y, -0.5+z$; (iii) $1.5-x, 0.5+y, 0.5-z$; (iv) $-x, 2-y, -z$.

dibasic thiophenedicarboxylate leads to simplification of the entire array. This concerns the elimination of three-connected nodes and an increased carboxylate/cluster ratio (3:1), which in effect increases the dimensionality of the carboxylate subconnectivity, existing in the form of a primitive cubic net (**pcu**, Schläfli point symbol $\{4^{12}.6^3\}$). The bipyridazine bridges did not generate additional intercluster links, but rather repeat the existing links already established by the TDC²⁻ bridges. In this way, four out of six topological links are doubled as a result of a concerted action of both sorts of the ligands (Figure 4). Two Cu^{II} ions adopt square-pyramidal environments (Addison parameters²⁶ τ are 0.23 for Cu1 and 0.22 for Cu2) (Table 4).

The structures of the two isotopic compounds, [Cu₅(μ-OH)₂{L}₄(L)₂(H₂O)₂·*n*H₂O (**4**: L = BDC²⁻, *n* = 5; **5**: L = HO-BDC²⁻, *n* = 6), are more complicated and they include pentanuclear net nodes (Figure 4). The present open-chain centrosymmetric Cu₅ units are unprecedented yet comprising a central trinuclear core [Cu₃(μ-OH)₂(pdz)₄] built up with two triple *bis*-pyridazino/hydroxo bridges, which itself is known for copper(II)¹³ and cobalt(II)¹⁰ pyridazine complexes. These

units are extended to the pentanuclear pattern by connecting two Cu₃ ions as annexes through carboxylate bridges and distal aqua ligands (Figure 5). These outer ions have a typically distorted [4+2] octahedral coordination, whereas the environment geometry of Cu₂ is close to a square pyramid with N₃ in the apex position, with Addison parameters²⁶ τ = 0.41 (**4a** at 296 K), τ = 0.37 (**4b** at 105 K) and τ = 0.42 (**5**) (Table 5).

The most striking features of the local coordination geometries are the appreciably compressed octahedral environments adopted by the central Cu^I ions lying on a centre of inversion. For both of the compounds, these involve two pairs of long “equatorial” Cu-N bonds (2.1733(18)-2.300(2) Å) accompanied by two very short “axial” Cu-O^I bonds (1.901(2)-1.9086(16) Å). The only documented example of the [Cu{(μ-OH)(μ-pdz)₂Cu₂}] pattern, in a 4,4'-bipyridazine complex, also implies such kind of a coordination octahedron adopted by the central Cu ion (Cu-O 1.887(2); Cu-N 2.146(2)-2.340(3) Å).¹³ Although these observations are suggestive of Jahn-Teller compression (indicating the unusual $\{d(z^2)\}$ electronic ground state of Cu^I ions), the present geometries much likely may be attributed to the dynamic disorder of an axis of Jahn-Teller elongation and consequent librational effects.³¹ First, the examination of the complex **4** at different temperatures (**4a**: 296 K, **4b**: 105 K, using the same single crystal) reveals an appreciable temperature dependence of the Cu^I-N bond lengths. Being actually equivalent at r.t. (2.221(2) × 2 and 2.252(2) × 2 Å), two pairs of the bonds became essentially differentiated upon cooling (2.1733(18) × 2 and 2.300(2) × 2 Å) (Table 5). Second, mean-square displacement amplitude (MSDA)³² analysis clearly indicates the presence of librational disorder involving all four Cu^I-N bonds, at both temperatures (for Cu^I-O1, Cu^I-N1 and Cu^I-N4 bonds, $\langle d^2 \rangle$ (×10⁴ Å²) = 11(11), 95(12) and 78(12) at 296K, and 9(8), 74(11) and 41(10) at 105 K, respectively), with the corresponding $\langle d^2 \rangle$ values being particularly high at r.t. Importantly, the bonds adopted by Cu₂ and Cu₃ ions are actually temperature invariant (Table 5). The application of such an approach towards “compressed” coordination geometry of Cu²⁺ ions was extensively discussed by Halcrow.³¹

The fact that the cluster units accommodate in total eight carboxylate and four pyridazine groups, allows a very high, up to twelve, connectivity at the net nodes.⁴ The latter is decreased in view of the generation of two double carboxylate links. This produces only a six-connected cluster/carboxylate subtopology (primitive cubic net), while the further cross-linking of the nodes by bipyridazine ligands yields a rarely encountered³³ uninodal ten-coordinated framework with a Schläfli point symbol $\{3^{12}.4^{28}.5^5\}$ (identified by a “**bct**” notation in the Reticular Chemistry Structure Resource database).³⁴

Magnetic properties

Compounds **1**, **3** and **4**, representing the cluster types **A**, **B** and **C**, respectively, were selected for an investigation of their magnetic properties. The $\chi_m T(T)$ plot of a polycrystalline sample of [Cu₂(μ-OH){TMA}(L)(H₂O)] (**1**) (scaled per Cu₂ unit) exhibits decreasing $\chi_m T$ values on cooling, starting with

Table 5 Selected bond distances (Å) and angles (°) for pentanuclear complexes **4** and **5**^a

[Cu ₅ (μ-OH) ₂ {BDC} ₄ (L) ₂ (H ₂ O) ₂]-5H ₂ O (4a , 296 K)			
Cu1-O1	1.9086(16) × 2	Cu3-O10 ^{iv}	1.9085(17)
Cu1-N1	2.221(2) × 2	Cu3-O6 ^v	1.9593(19)
Cu1-N4	2.252(2) × 2	Cu3-O7	1.9614(16)
		Cu3-O4	1.9685(18)
Cu2-O1	1.8800(17)	Cu3-O8	2.482(2)
Cu2-O3	1.9286(18)	Cu3-O2	2.733(2)
Cu2-O2	2.0040(18)		
Cu2-N2	2.195(2)		
Cu2-N3 ⁱⁱⁱ	2.224(2)		
[Cu ₅ (μ-OH) ₂ {BDC} ₄ (L) ₂ (H ₂ O) ₂]-5H ₂ O (4b , 105 K)			
Cu1-O1	1.9162(15) × 2	Cu3-O10 ^{iv}	1.9139(16)
Cu1-N1	2.300(2) × 2	Cu3-O6 ^v	1.9616(16)
Cu1-N4	2.1733(18) × 2	Cu3-O7	1.9615(14)
		Cu3-O4	1.9715(16)
Cu2-O1	1.8784(15)	Cu3-O8	2.4799(18)
Cu2-O3	1.9245(15)	Cu3-O2	2.7019(18)
Cu2-O2	2.0093(16)		
Cu2-N2	2.1671(19)		
Cu2-N3 ⁱⁱⁱ	2.227(2)		
[Cu ₅ (μ-OH) ₂ {HO-BDC} ₄ (L) ₂ (H ₂ O) ₂]-6H ₂ O (5)			
Cu1-O1	1.901(2) × 2	Cu3-O8	1.915(2)
Cu1-N1	2.138(3) × 2	Cu3-O6 ^{iv}	1.927(2)
Cu1-N4	2.344(3) × 2	Cu3-O4	1.949(2)
		Cu3-O10 ^v	1.964(2)
Cu2-O1	1.882(2)	Cu3-O11 ^v	2.541(3)
Cu2-O3	1.933(2)	Cu3-O2	2.667(3)
Cu2-O2	2.000(3)		
Cu2-N2	2.154(3)		
Cu2-N3 ⁱⁱⁱ	2.230(3)		

^a Symmetry codes for **4**: (iii) -0.5+x, -0.5-y, -0.5+z; (iv) -1+x, y, z; (v) -0.5-x, 0.5+y, 2.5-z. For **5**: (ii) x, 0.5-y, 0.5+z; (iv) -x, -0.5+y, 0.5-z; (v) 1+x, y, z.

0.91 cm³ K mol⁻¹ at 300 K and approaching a value of 0.05
 285 cm³ K mol⁻¹ at 1.9 K (Figure 6). This plot is typical for
 intracluster antiferromagnetic exchange interactions leading to
 a diamagnetic ground state. This behaviour may be compared
 with a simpler binuclear systems sustained by the mixed
 hydroxo + *syn-syn* carboxylate bridge between the Cu ions,
 290 which exhibit strong ferromagnetic coupling.³⁵ The small low
 temperature $\chi_m T$ value originates from a minor paramagnetic
 phase; this is reflected in the Curie tail as seen in the $\chi_m(T)$
 plot (Figure S24).

The inverse magnetic susceptibility curve (Figure S25)
 295 shows a linear behavior in the temperature range from 50 to
 300 K, which results in a Weiss constant $\theta = -37$ K, in good
 agreement with the negative slope of the $\chi_m T$ versus T curve.
 We can use the following isotropic Hamiltonian to describe
 the intracluster magnetic exchange interactions:

$$H = -2J(S_1 \cdot S_2)$$

The magnetic susceptibility data were least-squares fit to the
 Bleaney-Bowers equation³⁶ for isotropic exchange in the
 305 Cu(II) pair. A good simulation of the data is achieved with $J =$
 -17.5 cm⁻¹ ($g = 2.1$). The fact, that compound **1** shows a very
 complex bonding pattern with a heteroligand pyridazine/OH/
 carboxylate triple bridge connecting the two Cu(II) ions,
 prevents a detailed structure-property correlation, and thus the

310 experimentally determined J parameter comprises all possible
 exchange pathways between the spin centers.

The $\chi_m T(T)$ plot of a polycrystalline sample of [Cu₄(μ₃-
 OH)₂{TDC}₃(L)₂(H₂O)₂]-7H₂O (**3**) (scaled per Cu₄ unit)
 315 exhibits strongly decreasing $\chi_m T$ values on cooling, starting
 with 0.34 cm³ K mol⁻¹ at 300 K and approaching a zero value

$$H = -2J_1(S_2 \cdot S_{2i}) - 2J_2(S_1 \cdot S_2 + S_1 \cdot S_{2i} + S_2 \cdot S_{1i} + S_{2i} \cdot S_{1i}) \quad (1)$$

around 90 K (Figure 7). The high temperature $\chi_m T$ values are
 much smaller than the spin-only value of 1.5 cm³ K mol⁻¹ for
 four non-interacting spins with $S = 1/2$ ($g = 2.0$) which is due
 to strong intracluster antiferromagnetic exchange interactions.

320 The low temperature $\chi_m T$ values indicate a diamagnetic
 ground state of the tetranuclear complex.

Given the butterfly-type arrangement of the tetranuclear
 cluster fragment (Scheme 3) and leaving aside the asymmetry
 of the bonding pattern on the wings, we can use as an
 325 approximation which is justified below, the following
 isotropic Hamiltonian to describe the intracluster magnetic
 exchange interactions [equation (1)]:

This model approximates the [Cu₄] core with a rhombic
 symmetry while differentiating two magnetic exchange
 330 pathways, namely Cu2-Cu2ⁱ (J_1) vs Cu1-Cu2, Cu1-Cu2ⁱ,
 Cu2-Cu1ⁱ, Cu2ⁱ-Cu1ⁱ (J_2). Consequently, this Hamiltonian
 gives rise to six spin states comprising the total spin values
 (S_T) of 2, 1, 0 with the corresponding energy levels in terms of
 the magnetic coupling constants as given below:

$$335 E_1 (S_T = 2) = -\frac{1}{2} J_1 - 2 J_2$$

$$E_2 (S_T = 1) = -\frac{1}{2} J_1 + 2 J_2$$

$$E_3 (S_T = 1) = -\frac{1}{2} J_1$$

$$E_4 (S_T = 1) = +\frac{3}{2} J_1$$

$$340 E_5 (S_T = 0) = -\frac{1}{2} J_1 + 4 J_2$$

$$E_6 (S_T = 0) = +\frac{3}{2} J_1$$

$$\chi_m = 2N\beta^2 g^2 / kT \cdot (A/B); \quad (2)$$

$$A = 5\exp(-E_1/kT) + \exp(-E_2/kT) + \exp(-E_3/kT) + \exp(-E_4/kT)$$

$$B = 5\exp(-E_1/kT) + 3\exp(-E_2/kT) + 3\exp(-E_3/kT) + 3\exp(-E_4/kT) + \exp(-E_5/kT) + \exp(-E_6/kT)$$

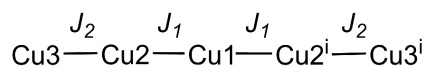
Applying these energy values to the van Vleck equation gives
 the following analytical expression [equation (2)]:

345 To reiterate at this stage, the linking pattern at the wing
 sides of the {Cu₄(μ₃-OH)₂} core differs since on two sides a
 chelating pyridazine is involved, a fact which would
 principally ask for two different exchange parameters, say J_2
 and J_3 . This would result in six energy levels in function of
 350 three J parameters.^{25b} However, in view of the rather smooth
 curve of the $\chi_m T(T)$ plot one can understand that any trials to
 fit the data to a three parameter model are not conclusive due
 to overparametrization. Next, it clearly turned out best to fix
 the J_1 parameter to a reasonable value of -110 cm⁻¹; this

355 coupling strength results from an analogous core structure^{25a}
and then using equation (2), the experimental data were fitted
satisfactorily in the temperature range 300–30 K with $J_2 = -$
228 cm⁻¹ ($g = 2.07$). Both values of the coupling constants
express the fairly strong antiferromagnetic intracuster
360 coupling which consequently results in a diamagnetic ground
state. One has to bear in mind, however, that the J_2 parameter
now represents an average coupling value on the wing sides.

The $\chi_m T(T)$ and $\chi_m(T)$ plots of a polycrystalline sample of
[Cu₅(μ-OH)₂{BDC}₄(L)₂(H₂O)₂]₅·5H₂O (**4**) (scaled per Cu₅
365 unit) are shown in Figure 8. The high-temperature $\chi_m T$ value
of 1.75 cm³ K mol⁻¹ is smaller than the spin-only value of 2.06
cm³ K mol⁻¹ for five non-interacting spins with $S = \frac{1}{2}$ ($g =$
2.2) and they decrease to a value approaching zero at 2K.
Both are indicative of strong antiferromagnetic exchange
370 interactions within the pentameric unit.

A structural analysis reveals that the central Cu₃ subunit
involves Cu1 bound to two equivalent inversion related Cu2
via two bridges, hydroxo and pyridazine. The pyridazine
bridges can be considered to be orthogonal connections,
375 because of the short-long bonds to Cu2 and Cu2' within each
pair. Cu-O connections to the bridging OH⁻ groups are short
and since the Cu-OH-Cu angle (114.3°) is large one would
anticipate strong antiferromagnetic exchange between Cu1
and the two Cu2 atoms through these bridges (equatorial-
380 equatorial connections). The Cu2-Cu3 connection is really
just a 1,3-carboxylate with short contacts to both copper
centers (the aqua O2 donor is just bonded to Cu2 with a short
contact, whereas the secondary Cu3-O2 interactions are only
very distal and weak, Table 6). Therefore both Cu2 atoms
385 are going to be antiferromagnetically coupled to Cu3, but with
a much smaller J value. The corresponding magnetic coupling
scheme is given as



and the isotropic Hamiltonian is

$$390 H = -2J_1(S_1 \cdot S_2 + S_1 \cdot S_{2i}) - 2J_2(S_2 \cdot S_3 + S_{2i} \cdot S_{3i})$$

The exchange model is therefore based on a strongly
antiferromagnetically coupled central linear trinuclear Cu₃
395 group, with the Cu3 centers weakly antiferromagnetically
coupled to the terminal coppers (Cu2) of the triad.

In the data fitting J_1 and J_2 were represented as a ratio
(J_1/J_2) and after varying the ratio, fitting the data, and
observing and minimizing the fitting coefficient a satisfactory
400 fit was obtained using MAGMUN4.11.³⁷ This programme
calculates the total spin states and their energies based on the
exchange Hamiltonian, and determines the fitted parameters
internally through weighted non-linear least squares
procedures. The optimum ratio was found to be $J_1/J_2 = 10$,
405 with the best fit parameters at $J_1 = -125(3)$ cm⁻¹, $J_2 = -12.5(3)$
cm⁻¹ and $g = 2.18$, providing the eminently sensible model
based on the regression statistics and the structure.

Thermal Stability

The thermal behavior of the compounds **1-5** was examined by
complementary TG/DTA-MS and temperature-dependent
powder X-ray diffractometry (TD PXRD) techniques. With
the exception of complex **4**, the stages of dehydration and
further weight losses due to the thermal destructions are not
separated and proceed above 150 °C, with the crystallization
of an inorganic product (CuO) observed above 350 °C.
415 Compound **1** is somewhat more stable. It does not show any
weight loss until a temperature of 260 °C. In the range 260-
340 °C, with a DTG peak maximum at 300 °C, it decomposes
(-29.7%) with dehydration (m/z 18) and release of CO₂ (m/z
44) due to decarboxylation. This is accompanied by loss of
420 crystallinity at 260 °C, as evidenced by PXRD patterns. The
stability of the aliphatic analog **2** is comparable. Dehydration
starts at 160 °C, and above 220 °C it was accompanied by
decarboxylation which results in one unresolved stage of
425 12.3% weight loss in the range of 160-270 °C (maximum at
250 °C). The PXRD patterns are also indicative for the
dehydration process (160-170 °C) since the interlayer spacing
is sensitive to elimination of the guest molecules located
between the coordination layers. Disintegration of the
430 structure was observed at 230 °C. Complex **3** experiences
partial dehydration above 60 °C, with release of 5 water
molecules in the temperature range of 60-170 °C (5.60%
observed; 5.82% calculated). This results in a phase transition
at 170 °C, and at 195 °C the compound gets amorphous due to
435 decomposition with release of CO₂. For the closely related **4**
and **5**, disintegration of the frameworks occurs at an identical
temperature of 235 °C. However, due to a more hydrophobic
nature of the isophthalate framework in **4**, vs. the 5-
hydroxyisophthalate analog **5**, the initial dehydration in the
440 first case proceeds more readily. The TG curve indicates two
insufficiently separated stages at 110-200 °C and 200-250 °C,
with a total weight loss of 7.3% corresponding to the release
of coordinated and outer sphere water molecules (calculated
7.32%). Further thermal decomposition proceeds at 270-340
445 °C. In the case of **5**, the dehydration begins at 160 °C.
Progressive release of water molecules (m/z 18) coincides
with beginning of decarboxylation (m/z 44) at 265 °C. The
weight loss of 8.5% in the temperature range 160-260 °C
corresponds to the elimination of 8 water molecules
450 (calculated 8.0%).

IR Spectra

The IR spectra of the complexes **1-5** exhibit strong and broad
absorption bands in the region of 3230-3500 cm⁻¹, which are
attributed to the ν(OH) vibrations of the aqua and hydroxo
455 ligands. Bands at 2850-2933 cm⁻¹ correspond to ν(CH)
vibrations of adamantane and aromatic moieties. The
absorptions for the carbonyl group, ν(CO), appear as very
strong bands at 1590-1627 cm⁻¹ (See Experimental section).
The absence of bands at 1730–1690 cm⁻¹, where ν(CO) of
460 COOH is expected to appear, confirms full deprotonation of
the polycarboxylate ligands in **1-5**.³⁸ Strong absorption bands
at 1358-1382 cm⁻¹ are characteristic for all the compounds,
they could be assigned to ν(CN) of the pyridazine rings.³⁹

Conclusions

The present results are important for providing innovative strategies for the construction of extended coordination lattices incorporating polynuclear metal-organic clusters. A combination of pyridazine, carboxylate and hydroxo ligands is especially well suited for sustaining coordination patterns of different nuclearities and connectivities: this kind of bridges reveals a perfect compatibility and they readily complement each other and act in a synergistic manner. In cooperation with μ -carboxylate and, especially μ -hydroxo groups, pyridazine typically behaves as short-distance diatomic bridge. Therefore, the present heteroligand system unites and extends the structural and functional potential of such common types of organic and inorganic bridges for the generation of discrete polynuclear arrangements of metal ions. At the same time, a multiplication of the ligand functionality, as it occurs for di- and tricarboxylate and bipyridazine ligands, allows the integration of the clusters into polymeric arrays, which could be anticipated for a broad range of transition metal ions and different kinds of organic linkers. Our study suggests also a new approach and attractive preparative sequence towards bridge-head heteroaryl C-functionalization of adamantane, which could find wider applications for the developing of multivalent geometrically rigid molecular building blocks incorporating "nanodiamond scaffolds".⁴⁰ Moreover, the study of magnetic properties of coordination network compounds is a very topical issue in the field of molecular magnetism.⁴¹ In the present case, the magnetic susceptibility data for clusters **1**, **3** and **4** reveal substantial antiferromagnetic coupling strengths, however with varying ratios of the coupling parameters. In particular, common to all three structure types **A**, **B** and **C** is the quite complex nature of bonding patterns including heteroligand multiple bridges connecting the spin centers which prevents a discussion of more detailed structure-property correlations.

Experimental

All starting materials were chemicals of reagent grade and used as received without further purification. Adamantane-1,3,5-tricarboxylic acid was synthesized in 62% yield by the Koch-Haaf carboxylation of 1,3,5-adamantanetriol with 100% HCOOH in a 15% oleum medium.⁴² The 1,2,4,5-tetrazine was prepared and freshly purified by sublimation as described previously.^{13,14c}

Synthesis of 1,3-bis(pyridazin-4-yl)adamantane (L) (Scheme 1). A solution of 1.24 g (15.1 mmol) 1,2,4,5-tetrazine and 1.26 g (6.8 mmol) 1,3-diethynyladamantane⁴³ in 40 ml of dry 1,4-dioxane was stirred at 90 °C over a period of 25 h. The reaction proceeded smoothly and the evolution of dinitrogen gas ceased after 15-16 h. The precipitate was filtered off, washed with 1,4-dioxane and diethyl ether and dried in air. It was dissolved in boiling methanol and the solution was decolorized by 15 min reflux with charcoal, then it was filtered and evaporated yielding 1.41 g (71%) of a colorless crystalline product. ¹H NMR (400 MHz, dmso-*d*₆): δ 9.38–9.28 (m, 2H), 9.06 (d, *J* = 5.4 Hz, 2H), 7.58 (dd, *J* = 5.5, 2.6 Hz, 2H), 2.42–2.32 (m, 2H), 2.10 (s, 2H), 1.98 (t, *J* = 3.7 Hz, 8H), 1.82 (d, *J* = 3.5 Hz, 2H). Anal. Calcd for C₁₈H₂₀N₄:

C, 73.94; H, 6.90; N, 19.17. Found: C, 74.06; H, 6.88; N, 19.04.

Preparation of the coordination compounds

The complexes were prepared under hydrothermal conditions as follows. A mixture of the starting compounds and distilled water were placed into a 20 mL Teflon-lined stainless steel autoclave, stirred for 10-30 min, and heated at 140 °C for 40-70 h in an oven, with further cooling to room temperature. In each the case, the excess of bipyridazine ligand was essential for partial hydrolysis of Cu(II) ions and generation of the desired hydroxo-bridged species. Under these conditions and absence of di- or tricarboxylate components, the reactions of Cu(OAc)₂·H₂O and bipyridazine ligand did not afford insoluble products.

Synthesis of [Cu₂(μ -OH){TMA}(L)(H₂O)] (1). A mixture of 6.8 mg (0.034 mmol) Cu(OAc)₂·H₂O, 3.1 mg (0.015 mmol) trimesic acid and 10.0 mg (0.034 mmol) ligand in a 1:0.44:1 molar ratio with 4 mL water was stirred for 30 min in a Teflon vessel, and then it was heated at 140 °C for 70 h. Slow cooling to r.t. over period of 48 h (cooling rate 2.5 °C h⁻¹) afforded a pure product as green prisms, which were washed with 3 mL of water and dried in air for 1 h (yield: 7.9 mg, 80%). Anal. Calcd for C₂₇H₂₆Cu₂N₄O₈: C, 49.01; H, 3.96; N, 8.47. Found: C, 48.89; H, 4.01; N, 8.35. IR (KBr discs, selected bands, cm⁻¹): 568w, 717s, 761m, 977w, 1022w, 1091w, 1359vs, 1407m, 1433s, 1558vs, 1607vs, 2852w, 2900m, 3233mbr, 3409m.

Synthesis of [Cu₄(μ ₃-OH)₂{ATC}₂(L)₂(H₂O)₂].H₂O (2). The compound was prepared in a similar manner, starting with 6.8 mg (0.034 mmol) Cu(OAc)₂·H₂O, 3.5 mg (0.013 mmol) adamantane-1,3,5-tricarboxylic acid, 10.0 mg (0.034 mmol) ligand (1:0.38:1 molar ratio) and 4 mL of water. Small green prismatic crystals of the product were obtained in 80% yield. Anal. Calcd for C₆₂H₇₈Cu₄N₈O₁₉: C, 49.86; H, 5.26; N, 7.50. Found: C, 50.03; H, 5.19; N, 7.59. IR (KBr discs, selected bands, cm⁻¹): 568w, 710m, 832w, 1084w, 1209w, 1274m, 1328s, 1358vs, 1442w, 1590vs, 2850m, 2930s, 3044m, 3269mbr, 3471mbr.

Synthesis of [Cu₄(μ ₃-OH)₂{TDC}₃(L)₂(H₂O)₂].7H₂O (3). An equimolar mixture of 5.0 mg (0.025 mmol) Cu(OAc)₂·H₂O, 4.3 mg (0.025 mmol) 2,5-thiophenedicarboxylic acid, 7.4 mg (0.025 mmol) ligand were placed in a Teflon vessel, and 5 mL of water was added. The mixture was stirred for 30 min and then it was heated at 140 °C for 24 h. Small blue prisms of pure product were obtained in 60% yield after slow cooling to r.t. for a period of 72 h. Anal. Calcd for C₅₄H₆₆Cu₄N₈O₂₃S₃: C, 41.96; H, 4.30; N, 7.25. Found: C, 42.11; H, 4.22; N, 7.37. IR (KBr discs, selected bands, cm⁻¹): 556w, 689w, 774m, 808w, 973w, 1022w, 1072w, 1111w, 1314s, 1358vs, 1452w, 1527s, 1561s, 1597vs, 2852m, 2913m, 3407sbr.

Synthesis of [Cu₅(μ -OH)₂{BDC}₄(L)₂(H₂O)₂].5H₂O (4). A mixture of 6.8 mg (0.034 mmol) Cu(OAc)₂·H₂O, 5.7 mg (0.034 mmol) isophthalic acid, 10.0 mg (0.034 mmol) ligand, all in an equimolar ratio, and 4 mL of water was stirred for 10 min and then heated at 140 °C for 24 h in a Teflon vessel. After cooling to r.t. for a period of 72 h, large blue-green crystals of the pure product were collected by filtration (yield:

Table 6 Crystal data for [Cu₂(μ-OH){TMA}(L)(H₂O)] (**1**), [Cu₄(μ₃-OH)₂{ATC}₂(L)₂(H₂O)₂·H₂O (**2**), [Cu₄(μ₃-OH)₂{TDC}₃(L)₂(H₂O)₂·7H₂O (**3**), [Cu₅(μ-OH)₂{BDC}₄(L)₂(H₂O)₂·5H₂O (**4a** and **4b**) and [Cu₅(μ-OH)₂{HO-BDC}₄(L)₂(H₂O)₂·6H₂O (**5**)

	1	2	3	4a	4b	5
Formula	C ₂₇ H ₂₆ Cu ₂ N ₄ O ₈	C ₆₂ H ₇₈ Cu ₄ N ₈ O ₁₉	C ₅₄ H ₆₆ Cu ₄ N ₈ O ₂₃ S ₃	C ₆₈ H ₇₂ Cu ₅ N ₈ O ₂₅	C ₆₈ H ₇₂ Cu ₅ N ₈ O ₂₅	C ₆₈ H ₇₄ Cu ₅ N ₈ O ₃₀
<i>T</i> , K	213	296	173	296	105	296
<i>M</i>	661.60	1493.48	1545.49	1719.04	1719.04	1801.05
Crystal system	Monoclinic	Triclinic	Monoclinic	Monoclinic	Monoclinic	Monoclinic
Space group, <i>Z</i>	<i>C</i> 2/ <i>c</i> , 8	<i>P</i> 1, 1	<i>P</i> 2 ₁ / <i>n</i> , 2	<i>P</i> 2 ₁ / <i>n</i> , 2	<i>P</i> 2 ₁ / <i>n</i> , 2	<i>P</i> 2 ₁ / <i>c</i> , 2
<i>a</i> / Å	24.8536(18)	11.1208(9)	13.3933(4)	10.0517(7)	10.0322(6)	10.0552(5)
<i>b</i> / Å	10.8716(7)	11.5078(10)	9.9035(3)	18.4855(9)	18.4439(9)	18.7840(8)
<i>c</i> / Å	18.6837(14)	13.8841(13)	23.7661(8)	19.1143(13)	19.0354(12)	19.1757(9)
α	90	83.981(6)	90	90	90	90
β	101.581(8)	67.507(6)	98.036(2)	104.721(5)	104.897(5)	104.829(2)
γ	90	62.065(5)	90	90	90	90
<i>V</i> / Å ³	4945.5(6)	1444.3(2)	3121.39(17)	3435.1(4)	3403.8(3)	3501.2(3)
μ (Mo-K α)/ mm ⁻¹	1.783	1.541	1.530	1.613	1.627	1.591
<i>D</i> _c / g cm ⁻³	1.777	1.717	1.644	1.662	1.677	1.708
θ_{\max} / °	25.96	26.94	27.10	28.54	28.54	27.48
Meas/ Unique reflns	16964/ 4789	15505/ 6248	29009/ 6862	28251/ 8582	29556/ 8509	31226/ 8020
<i>R</i> _{int}	0.041	0.061	0.085	0.042	0.046	0.088
Parameters refined	433	419	477	502	502	502
<i>R</i> 1 [<i>I</i> > 2 σ (<i>I</i>)]	0.033	0.055	0.049	0.036	0.032	0.047
<i>wR</i> 2 [all data]	0.084	0.098	0.104	0.095	0.081	0.104
Goof on <i>F</i> ²	0.917	0.916	0.990	0.965	0.901	1.010
Max, min peak/ e Å ⁻³	0.44, -0.78	0.58, -0.59	0.59, -0.51	0.64, -1.10	0.54, -0.55	0.47, -0.53

9.3 mg, or 80%, based on Cu). Anal. Calcd for
 580 C₆₈H₇₂Cu₅N₈O₂₅: C, 47.51; H, 4.22; N, 6.52. Found: C, 47.59;
 H, 4.19; N, 6.63. IR (KBr discs, selected bands, cm⁻¹): 548w,
 716m, 748m, 806w, 1084w, 1156w, 1268w, 1368s, 1390vs,
 1450m, 1476w, 1560s, 1622vs, 2856m, 2922m, 3400sbr,
 3456sbr.

585 **Synthesis of [Cu₅(μ-OH)₂{HO-BDC}₄(L)₂(H₂O)₂·6H₂O**
(5). The compound was prepared similarly as for **4** from a
 mixture of 6.8 mg (0.034 mmol) Cu(OAc)₂·H₂O, 6.2 mg
 620 (0.034 mmol) 5-hydroxyisophthalic acid and 10.0 mg (0.034
 mmol) ligand, giving large blue-green prisms (yield 75%).
 590 Anal. Calcd for C₆₈H₇₄Cu₅N₈O₃₀: C, 45.34; H, 4.14; N, 6.22.
 Found: C, 45.47; H, 4.13; N, 6.39. IR (KBr discs, selected
 bands, cm⁻¹): 558w, 646w, 678w, 721s, 777s, 985m, 1001m,
 1021m, 1102w, 1128w, 1195m, 1218w, 1265m, 1280m,
 1296m, 1382vs, 1420s, 1449m, 1472m, 1545s, 1593s, 1627s,
 595 2856m, 2899m, 2933s, 3370sbr, 3500s, 3586m.

Measurements

Thermogravimetric/differential thermal analysis mass
 spectrometry (TG/DTA-MS) was performed on a Netzsch F1
 Jupiter device connected to an Aeolos mass spectrometer. The
 600 sample was heated at a rate of 10° min⁻¹. The temperature-
 dependent X-ray measurements were carried out on a Stoe
 STADIP with a high-temperature attachment and image-plate
 detector system. PXRD was carried out on a Stoe STADIP
 (Cu K α) using a linear PSD detector and on a Shimadzu
 605 XRD-6000 (Cu K α radiation). Elemental analysis was carried
 out with a Vario EL-Heraeus microanalyzer. IR spectra
 (400–4000 cm⁻¹, KBr disks) were collected using a Perkin-
 Elmer FTIR spectrometer.

Magnetic susceptibility measurements were made on a
 610 Quantum Design MPMS SQUID-XL magnetometer under an
 applied magnetic field of 10³ Oe between 300 and 1.9 K. The
 samples were prepared in a gelatine capsule. Diamagnetic

corrections were made for the samples using the
 approximation -0.45 × molecular weight × 10⁻⁶ cm³ mol⁻¹ and
 615 the sample holder was corrected for by measuring directly the
 susceptibility of the empty capsule.

X-Ray crystallography

The diffraction data were collected with graphite-
 monochromated Mo-K α radiation (λ = 0.71073 Å) (Table 6).
 620 Measurements for **1** at 213 K and for **4** (**4a**: 296 K, **4b**: 105 K)
 were made using a Stoe Image Plate Diffraction System, φ
 oscillation scans (numerical absorption correction using X-
 RED and X-SHAPE).⁴⁴ Measurements for **2**, **3** and **5** were
 625 performed at 173 K on a Bruker APEXII CCD area-detector
 diffractometer (ω scans). The data were corrected for Lorentz-
 polarization effects and for the effects of absorption (multi-
 scans method). The structures were solved by direct methods
 and refined by full-matrix least-squares on *F*² using the
 SHELX-97 package.⁴⁵ The CH-hydrogen atoms were added
 630 geometrically, with *U*_{iso} = 1.2*U*_{eq}(C) and OH-hydrogen atoms
 were located and included with fixed *d* (O-H) = 0.85 Å and
*U*_{iso} = 1.5*U*_{eq}(O). Part of the solvate water molecules in **2-4**
 are disordered. They were refined anisotropically and the
 635 hydrogen atoms were not added. In **1**, the binuclear cluster is
 equally disordered over two positions (Cu ion, μ-OH and aqua
 ligand; one of the pyridazine cycles is also disordered
 adopting two orientations). Attempted refinements in space
 groups of lower symmetry did not afford an ordered model.
 This fragment was freely refined anisotropically and the
 640 hydrogen atoms were added as stated above with partial
 contributions of 0.5. In **3**, one of the TDC²⁻ ligands is equally
 disordered over two positions across a center of inversion.
 The disorder was resolved without restraints in geometry, but
 with restrained parameters for thermal motion of the carbon
 645 atoms. The topological analysis was performed using TOPOS

4.0⁴⁶ and Graphical visualization of the structures was made using the program Diamond 2.1e.⁴⁷

CCDC reference numbers 967343-967348.

For crystallographic data in CIF or other electronic format see DOI: ...

Acknowledgements

Financial support by Deutsche Forschungsgemeinschaft, grant KR 1675/4-3 (HK and KVD) and by the Swiss National Science Foundation (grant 200020-130266) is gratefully acknowledged.

References

- D. J. Tranchemontagne, J. L. Mendoza-Cortés, M. O'Keeffe and O. M. Yaghi, *Chem. Soc. Rev.*, 2009, **38**, 1257; J. J. Perry IV, J. A. Perman and M. J. Zaworotko, *Chem. Soc. Rev.*, 2009, **38**, 1400; H. Furukawa, N. Ko, Y. B. Go, N. Aratani, S. B. Choi, E. Choi, A. O. Yazaydin, R. Q. Snurr, M. O'Keeffe, J. Kim and O. M. Yaghi, *Science*, 2010, **329**, 424; J. Kim, B. Chen, T. M. Reincke, H. Li, M. Eddaoudi, D. B. Moler, M. O'Keeffe and O. M. Yaghi, *J. Am. Chem. Soc.*, 2001, **123**, 8239.
- M. O'Keeffe, M. A. Peskov, S. J. Ramsden and O. M. Yaghi, *Acc. Chem. Res.*, 2008, **41**, 1782.
- P. Hubberstey, X. Lin, N. R. Champness and M. Schröder, in *Metal-Organic Frameworks: Design and Applications*; John Wiley & Sons, Inc.: Hoboken, New Jersey, 2010.
- Q. Lin, T. Wu, X. Bu and P. Feng, *Dalton Trans.*, 2012, **41**, 3620; J. Jia, X. Lin, C. Wilson, A. J. Blake, N. R. Champness, P. Hubberstey, G. Walker, E. J. Cussen and M. Schröder, *Chem. Commun.*, 2007, 840; G.-H. Cui, C.-H. He, C.-J. Jiao, J.-C. Geng and V. A. Blatov, *CrystEngComm*, 2012, **14**, 4210; X.-M. Zhang, R.-Q. Fang and H.-S. Wu, *J. Am. Chem. Soc.*, 2005, **127**, 7670; D. Li, T. Wu, X.-P. Zhou, R. Zhou and X.-C. Huang, *Angew. Chem. Int. Ed.*, 2005, **44**, 4175; J. H. Cavka, S. Jakobsen, U. Olsbye, N. Guillou, C. Lamberti, S. Bordiga and K. P. Lillerud, *J. Am. Chem. Soc.*, 2008, **130**, 13850.
- C. Janiak, *Dalton Trans.*, 2003, 2781.
- C. Heering, I. Boldog, V. Vasylyeva, J. Sanchiz and C. Janiak, *CrystEngComm*, 2013, **15**, 9757.
- B. Gil-Hernández, P. Gili, J. K. Vieth, C. Janiak and J. Sanchiz, *Inorg. Chem.*, 2010, **49**, 7478; J. K. Maclaren, J. Sanchiz, P. Gilib and C. Janiak, *New J. Chem.*, 2012, **36**, 1596; H. H. Monfared, J. Sanchiz, Z. Kalantari and C. Janiak, *Inorg. Chim. Acta*, 2009, **362**, 3791.
- F. A. Almeida Paz, J. Klinowski, S. M. F. Vilela, J. P. C. Tomé, J. A. S. Cavaleiro and J. Rocha, *Chem. Soc. Rev.*, 2012, **41**, 1088; D. Zhao, D. J. Timmons, D. Yuan and H.-C. Zhou, *Acc. Chem. Res.*, 2011, **44**, 123.
- S. S. Tandon, L. K. Thompson and R. C. Hynes, *Inorg. Chem.*, 1992, **31**, 2210; C. Li, N. Kanehisa, Y. Miyagi, Y. Nakao, S. Takamizawa, W. Mori and Y. Kai, *Bull. Chem. Soc. Jpn.*, 1997, **70**, 2429.
- T. Yi, C. Ho-Chol, S. Gao and S. Kitagawa, *Eur. J. Inorg. Chem.*, 2006, 1381.
- A.-C. Knall and C. Slugovc, *Chem. Soc. Rev.*, 2013, **42**, 5131.
- A. T. M. Marcelis and H. C. van der Plas, *J. Heterocyclic Chem.* 1987, **24**, 545; J. Sauer, D. K. Heldmann, J. Hetzenegger, J. Krauthan, H. Sichert and J. Schuster, *Eur. J. Org. Chem.*, 1998, 2885.
- K. V. Domasevitch, I. A. Gural'skiy, P. V. Solntsev, E. B. Rusanov, H. Krautscheid, J. A. K. Howard and A. N. Chernega, *Dalton Trans.*, 2007, 3140.
- (a) I. A. Gural'skiy, P. V. Solntsev, H. Krautscheid and K. V. Domasevitch, *Chem. Commun.*, 2006, 4808; (b) K. V. Domasevitch, P. V. Solntsev, I. A. Gural'skiy, H. Krautscheid, E. B. Rusanov, A. N. Chernega and J. A. K. Howard, *Dalton Trans.*, 2007, 3893; (c) A. S. Degtyarenko, P. V. Solntsev, H. Krautscheid, E. B. Rusanov, A. N. Chernega and K. V. Domasevitch, *New J. Chem.*, 2008, **32**, 1910.
- T. Otieno, S. J. Rettig, R. C. Thompson and J. Trotter, *Inorg. Chem.*, 1995, **34**, 1718.
- K. V. Domasevitch, J. A. Rusanova, I. A. Gural'skiy and P. V. Solntsev, *Acta Crystallogr., Sect. C: Cryst. Struct. Commun.*, 2012, **68**, m295.
- C. Näther and I. Jeß, *Inorg. Chem.*, 2003, **42**, 2968; P. V. Solntsev, J. Sieler, H. Krautscheid and K. V. Domasevitch, *Dalton Trans.*, 2004, 1153; K. V. Domasevitch, P. V. Solntsev, H. Krautscheid, I. S. Zhlyenko, E. B. Rusanov and A. N. Chernega, *Chem. Commun.*, 2012, **48**, 5847; L. Plasseraud, H. Maid, F. Hampel and R. W. Saalfrank, *Chem. - Eur. J.*, 2001, **7**, 4007; A. S. Batsanov, M. Begley, M. W. George, P. Hubberstey, M. Munakata, C. Russell and P. H. Walton, *J. Chem. Soc. Dalton Trans.*, 1999, 4251; M. Maekawa, M. Munakata, T. Kuroda-Sowa and Y. Nozaka, *J. Chem. Soc. Dalton Trans.*, 1994, 603; M. J. Begley, P. Hubberstey, C. E. Russell and P. H. Walton, *J. Chem. Soc. Dalton Trans.*, 1994, 2483; D. Hagman, C. Sangregorio, C. J. O'Connor and J. Zubeita, *J. Chem. Soc. Dalton Trans.*, 1998, 3707.
- F. Lloret, G. De Munno, M. Julve, J. Cano, R. Ruiz and A. Caneschi, *Angew. Chem. Int. Ed.*, 1998, **37**, 135; A. Escuer, F.A. Mautner, N. Sanz and R. Vicente, *Inorg. Chim. Acta*, 2002, **340**, 163; T. Otieno, S. J. Rettig, R. C. Thompson and J. Trotter, *Acta Crystallogr., Sect. C: Cryst. Struct. Commun.*, 1993, **49**, 2067; L. Pazderski, E. Szlyk, A. Wojtczak, L. Kozerski and J. Sitkowski, *Acta Crystallogr., Sect. E: Struct. Rep. Online*, 2004, **60**, 1270; E. Krupicka and A. Lentz, *Z. Kristallogr.-New Cryst. Struct.*, 2001, **216**, 289; A. S. Degtyarenko and K. V. Domasevitch, *Acta Crystallogr., Sect. C: Cryst. Struct. Commun.*, 2013, **69**, 219.
- Carlucci, L.; Ciani, G.; Moret, M.; Sironi, A. *J. Chem. Soc. Dalton Trans.* 1994, 2397.
- (a) T. Fetzter, A. Lentz, T. Debaerdemaeker and O. Abou-El-Wafa, *Z. Naturforsch., Teil B*, 1990, **45**, 199; (b) L. Pazderski, E. Szlyk, A. Wojtczak, L. Kozerski, J. Sitkowski and B. Kamieński, *J. Mol. Struct.*, 2004, **697**, 143.
- J. Cano, G. De Munno, F. Lloret and M. Julve, *Inorg. Chem.*, 2000, **39**, 1611.
- T. V. Yilmaz, E. Senel and C. Kazak, *Aust. J. Chem.*, 2008, **61**, 634.
- K. Hyde, G. F. Kokoszka and G. Gordon, *J. Inorg. Nucl. Chem.*, 1969, **31**, 1993; J. R. Ferraro, J. Zipper and W. Wozniak, *Appl. Spectrosc.*, 1969, **23**, 160; J. R. Allan, G. A. Barnes and D. H. Brown, *J. Inorg. Nucl. Chem.*, 1971, **33**, 3765; S. Emori, M. Inoue and M. Kubo, *Bull. Chem. Soc. Jpn.*, 1972, **45**, 2259.
- C. B. Aakeröy, N. R. Champness and C. Janiak, *CrystEngComm*, 2010, **12**, 22; B. Wisser, Y. Lu and C. Janiak, *Z. Anorg. Allg. Chem.*, 2007, **633**, 1189; H. A. Habib, A. Hoffmann, H. A. Höpfe and C. Janiak, *Dalton Trans.*, 2009, 1742; H. A. Habib, J. Sanchiz and C. Janiak, *Dalton Trans.*, 2008, 1734.
- (a) G. A. Senchyk, A. B. Lysenko, H. Krautscheid, E. B. Rusanov, A. N. Chernega, K. W. Krämer, S.-X. Liu, S. Decurtins and K. V. Domasevitch, *Inorg. Chem.*, 2013, **52**, 863; (b) H. A. Habib, J. Sanchiz and C. Janiak, *Inorg. Chim. Acta*, 2009, **362**, 2452; (c) G. A. Senchyk, A. B. Lysenko, H. Krautscheid, J. Sieler and K. V. Domasevitch, *Acta Crystallogr., Sect. C: Cryst. Struct. Commun.*, 2008, **64**, m246.
- A. W. Addison, T. N. Rao, J. Reedijk, J. van Rijn and G. C. Verschoor, *J. Chem. Soc. Dalton Trans.*, 1984, 1349.
- V. A. Blatov, L. Carlucci, G. Ciani and D. M. Proserpio, *CrystEngComm*, 2004, **6**, 378.
- I. A. Baburin, V. A. Blatov, L. Carlucci, G. Ciani and D. M. Proserpio, *J. Solid State Chem.*, 2005, **178**, 2452; I. A. Baburin, V. A. Blatov, L. Carlucci, G. Ciani and D. M. Proserpio, *CrystEngComm*, 2008, **10**, 1822; I. A. Baburin, V. A. Blatov, L. Carlucci, G. Ciani and D. M. Proserpio, *Cryst. Growth Des.*, 2008, **8**, 519.
- S. S. Chui, S. M. Lo, J. P. Charmant, A. G. Orpen and I. D. Williams, *Science*, 1999, **283**, 1148; L. Alaerts, E. Séguin, H. Poelman, F. Thibault-Starzyk, P. A. Jacobs and D. E. D. Vos, *Chem. - Eur. J.*, 2006, **12**, 7353.
- G.-X. Liu, K. Zhu, H. Chen, R.-Y. Huang, H. Xu and X.-M. Ren, *Inorg. Chim. Acta*, 2009, **362**, 1605; K.-H. He, Y.-W. Li, Y.-Q. Chen, W.-C. Song and X.-H. Bu, *Cryst. Growth Des.*, 2012, **12**, 2730; H. Li, W. Shi, K. Zhao, Zh. Niu, H. Li and P. Cheng, *Chem. - Eur. J.*, 2013, **19**, 3358; H.-H. Li, W. Shi, N. Xu, Zh.-J. Zhang, Zh. Niu, T. Han and P. Cheng, *Cryst. Growth Des.*, 2012, **12**, 2602.

- 31 M. A. Halcrow, *Dalton Trans.*, 2003, 4375; M. A. Halcrow, *Chem. Soc. Rev.*, 2013, **42**, 1784.
- 32 L. R. Falvello, *J. Chem. Soc., Dalton Trans.*, 1997, 4463; J. D. 855
785 Dunitz, V. Schomaker and K. N. Trueblood, *J. Phys. Chem.*, 1988, **92**, 856.
- 33 W.-C. Song, Q. Pan, P.-C. Song, Q. Zhao, Y.-F. Zeng, T.-L. Hu and X.-H. Bu, *Chem. Commun.*, 2010, **46**, 4890.
- 34 (a) Reticular Chemistry Structure Resource (RCSR), 860
790 <http://rcsr.anu.edu.au>; (b) V. A. Blatov and A. P. Shevchenko, *TOPOS 4.0*, Samara State University, Russia, 1999.
- 35 H. A. Habib, J. Sanchiz and C. Janiak, *Dalton Trans.*, 2008, 4877.
- 36 B. Bleaney and K. D. Bowers, *Proc. Roy. Soc. (London) Ser. A*, 1952, **214**, 451. 865
795
- 37 MAGMUN4.11/OW01.exe is available as a combined package free of charge from the authors (<http://www.ucs.mun.ca/~lthomp/magmun>). MAGMUN was developed by Dr. Zh. Xu (Memorial University), and OW01.exe by Dr. O. Waldmann.
- 38 W. Brzyska and P. Sadowski, *Pol. J. Chem.*, 1987, **61**, 273; W. 870
800 Brzyska and W. Wolodkiewicz, *Pol. J. Chem.*, 1986, **60**, 697; K. Wieghardt, *J. Chem. Soc., Dalton Trans.*, 1973, 2548; L. J. Bellamy, *The Infrared Spectra of Complex Molecules* Wiley, New York, 1958.
- 39 S. Breda, I. D. Reva, L. Lapinski, M. J. Nowak and R. Fausto, *J. Mol. Struct.*, 2006, **786**, 193; J. Vázquez, J. J. L. Gozález, F. Márquez 875
805 and J. E. Boggs, *J. Raman Spectr.*, 1998, **29**, 547.
- 40 M. A. Gunawan, J.-C. Hierso, D. Poinsot, A. A. Fokin, N. A. Fokina, B. A. Tkachenko and P. R. Schreiner, *New. J. Chem.*, 2014, **38**, 28.
- 41 (a) O. Kahn, *Molecular Magnetism*; VCH: Weinheim, Gemany, 1993. (b) L. K. Thompson (Ed.), *Magnetism: Molecular and 880
810 Supramolecular Perspectives; Coord. Chem. Rev.*, 2005, **249**, 2549; (c) F. Bonadio, M.-C. Senna, J. Enslin, A. Sieber, A. Neels, H. Stoeckli-Evans and S. Decurtins, *Inorg. Chem.*, 2005, **44**, 969; (d) M. Pilkington and S. Decurtins, *Chimia*, 2000, **54**, 593.
- 42 G. A. Senchyk, A. B. Lysenko, I. Boldog, E. B. Rusanov, A. N. 885
815 Chernega, H. Krautscheid and K. V. Domasevitch, *Dalton Trans.*, 2012, **41**, 8675.
- 43 T. G. Archibald, A. A. Malik and K. Baum, *Macromolecules*, 1991, **24**, 5261.
- 44 (a) Stoe & Cie, *X-SHAPE*, Revision 1.06, Stoe & Cie GmbH, 890
820 Darmstadt, Germany, 1999; (b) Stoe & Cie, *X-RED*, Version 1.22, Stoe & Cie GmbH, Darmstadt, Germany, 2001.
- 45 G. M. Sheldrick, *Acta Crystallogr., Sect. A: Found. Crystallogr.*, 1990, **46**, 467; G. M. Sheldrick, *Acta Crystallogr., Sect. A: Found. 895
900 Crystallogr.*, 2008, **64**, 112.
- 825 46 V. A. Blatov, *TOPOS, IUCr CompComm Newsletter*, 2006, **7**, 4; V. A. Blatov, A. P. Shevchenko and V. N. Serezhkin, *J. Appl. Crystallogr.*, 2000, **33**, 1193.
- 47 K. Brandenburg, *Diamond 2.1e*, Crystal Impact GbR, Bonn, 1999. 900
830
905
835
910
840
915
845
920
850

925

SCHEME and FIGURE CAPTIONS

990

930 **Scheme 1** Synthesis of the bis-pyridazine ligand by a stepwise functionalization of the adamantane core.

Scheme 2 Three kinds of polynuclear Cu/OH/pyridazine clusters, representing the structures of the reported complexes: **A** – binuclear motif in **1**; **B** – tetranuclear clusters in **2** and **3**; **C** – pentanuclear units in **4** and 935 **5**, with a central trinuclear hydroxo/pyridazine core.

995

Scheme 3 $\{\text{Cu}_4(\mu_3\text{-OH})_2\}$ core fragment of **3** and the corresponding magnetic coupling scheme.

940

Fig. 1 (a) Binuclear cluster in the environment of carboxylate and pyridazine ligands in the structure of **1**; (b) 2D Cu/carboxylate subtopology in the form of hexagonal net, with the pyridazine-N donors accommodated at two sides of the plane. Only one orientation of the 945 disordered cluster is shown.

1000

Fig. 2 Interpenetration of two inversion-related 3D frameworks (marked with blue and grey bonds) in the structure of **1**. The hydroxocopper-carboxylate layers are orthogonal to the drawing plane.

1005

950

Fig. 3 (a) Tetranuclear cluster in **2** showing the hydrogen bonding interactions with $\mu_3\text{-OH}$ and aqua ligands; (b) Cu/carboxylate topology in the form of six- and three-connected CdI_2 -like network. Note the intrinsic topological significance of the tricarboxylate linker. Symmetry codes: (i) 955 $-x, 2-y, 1-z$; (ii) $-1+x, y, z$; (iii) $1-x, 1-y, 1-z$; (iv) $x, y, -1+z$.

1010

Fig. 4 (a) Primitive cubic framework of **3** viewed down the b direction showing interconnection of heteroligand carboxylate/pyridazine planes by additional carboxylate linkers; (b) The heteroligand planes with double 960 organic bridges between the tetranuclear clusters constituting the framework nodes.

1015

Fig. 5 (a) Pentanuclear centrosymmetric clusters observed in **4** and **5**. Note the compressed octahedral geometry around Cu1 ion. (b) Mode of 965 interconnection of the clusters by dicarboxylate links. Symmetry codes: (i) $-x, -y, 2-z$; (ii) $0.5-x, 0.5+y, 2.5-z$; (iii) $-0.5+x, -0.5-y, -0.5+z$; (iv) $-1+x, y, z$; (v) $-0.5-x, 0.5+y, 2.5-z$.

Fig. 6 Thermal variation of $\chi_m T$ for **1** (the solid line is drawn based on the 970 Bleaney-Bowers equation).

1020

Fig. 7 Thermal variation of $\chi_m T$ for **3** (solid line is a fit according to equation 1).

975 **Fig. 8** Thermal variation of χ_m and $\chi_m T$ for **4** (the solid lines are a fit to the data).

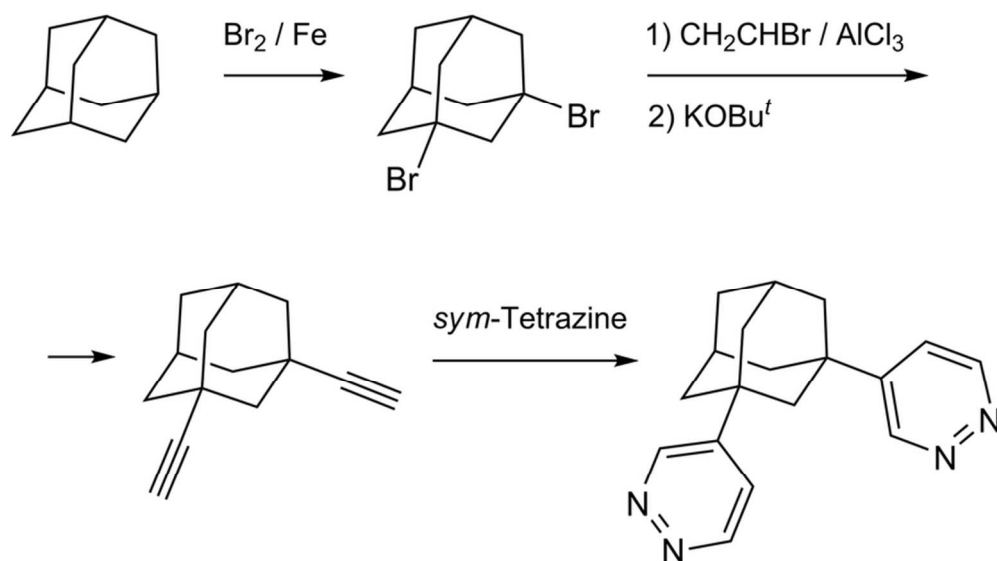
1025

Graphical contents entry

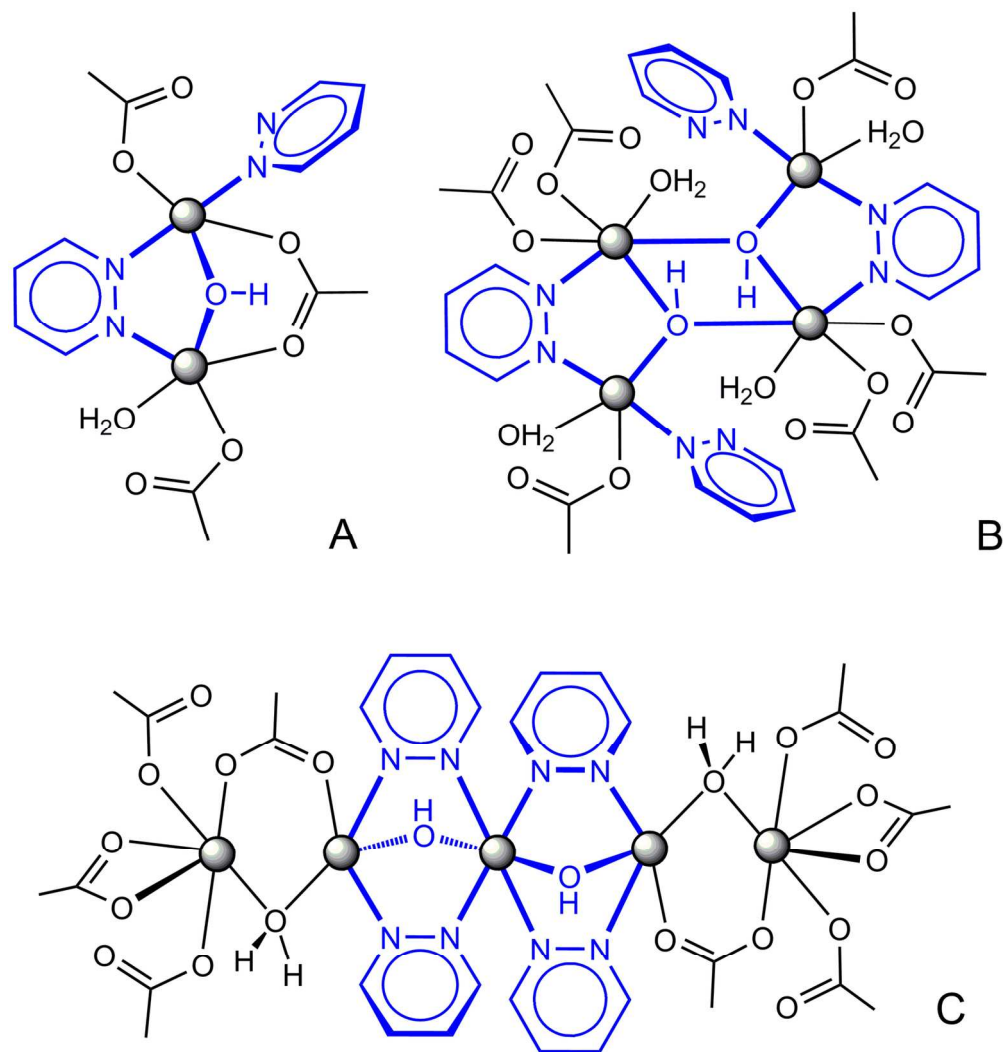
980

1030

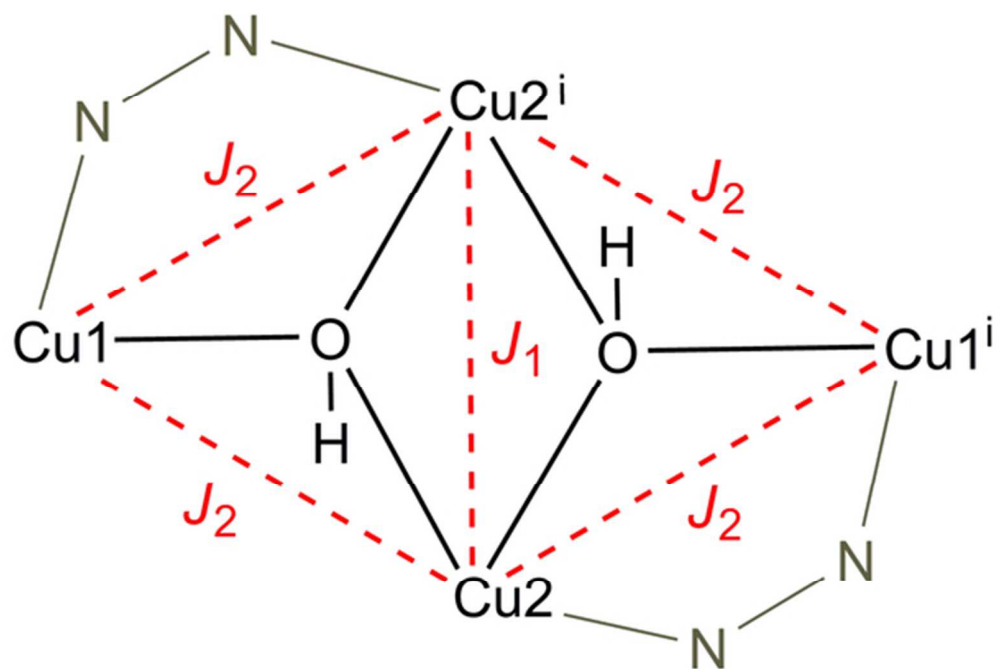
Three types of polynuclear Cu(II) clusters rely on a compatibility of short-distance hydroxo-, carboxylato and pyridazine bridges and are applicable for the construction 985 of 3D MOF structures incorporating complementary set of polyfunctional organic links.



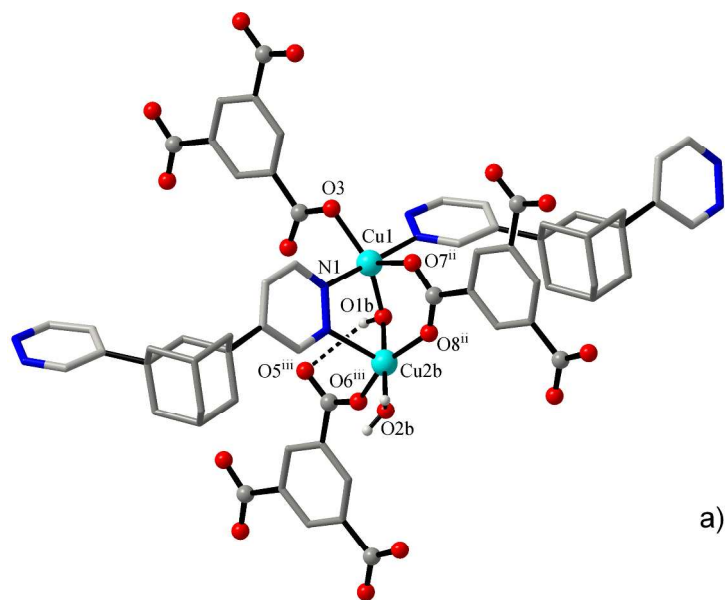
Synthesis of the bis-pyridazine ligand by a stepwise functionalization of the adamantane core.
77x43mm (300 x 300 DPI)



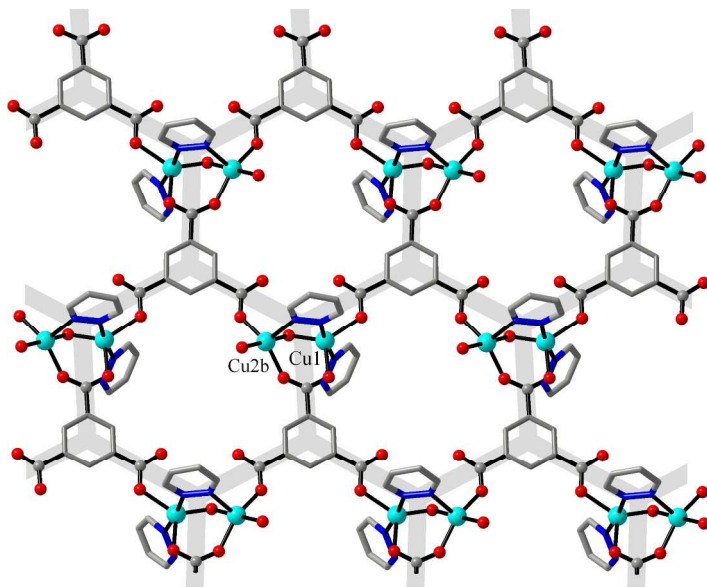
Three kinds of polynuclear Cu/OH/pyridazine clusters, representing the structures of the reported complexes: A – binuclear motif in 1; B – tetranuclear clusters in 2 and 3; C – pentanuclear units in 4 and 5, with a central trinuclear hydroxo/pyridazine core.
146x154mm (300 x 300 DPI)



{Cu₄(μ₃-OH)₂} core fragment of 3 and the corresponding magnetic coupling scheme.
51x35mm (300 x 300 DPI)

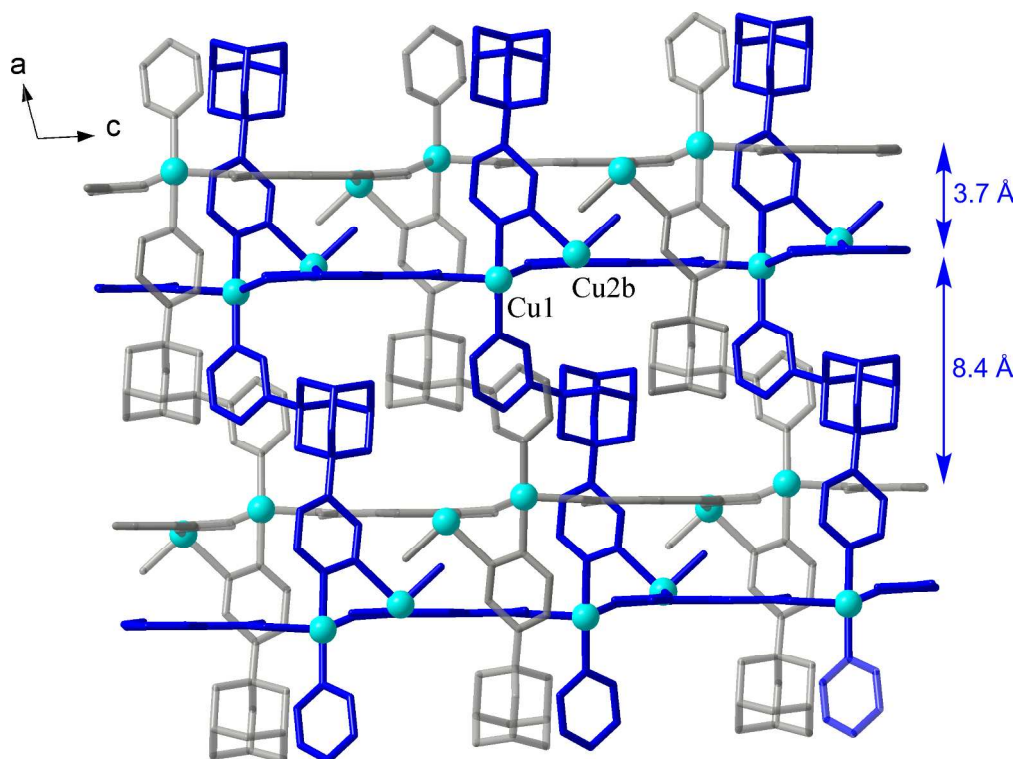


a)

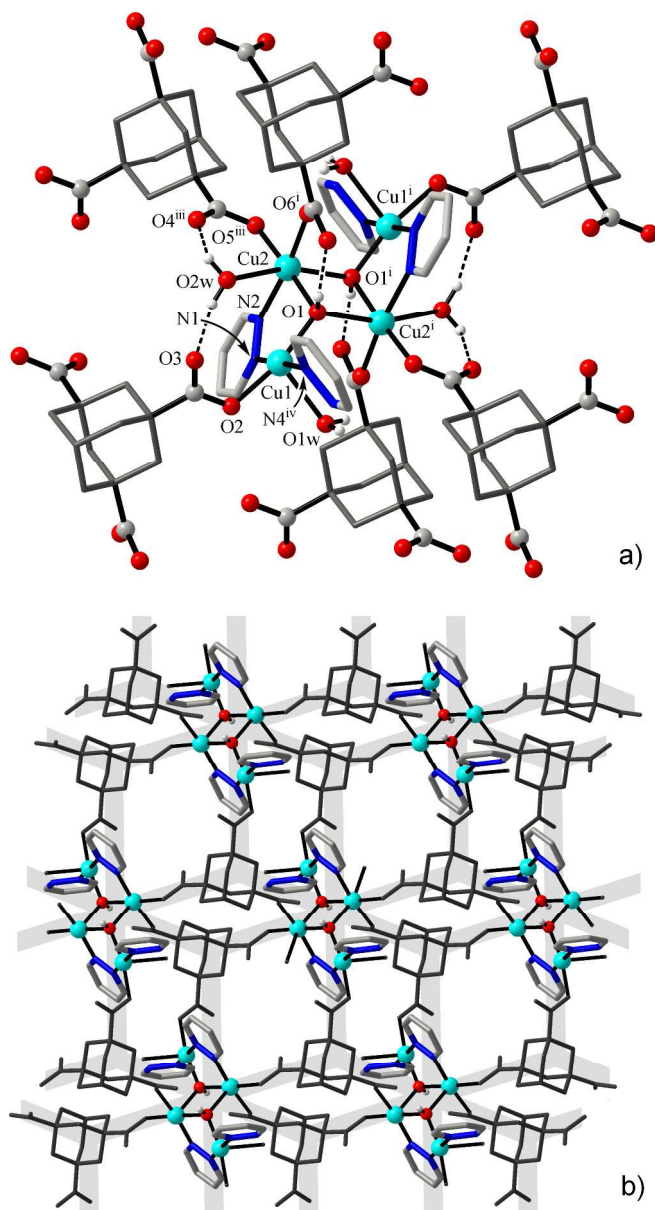


b)

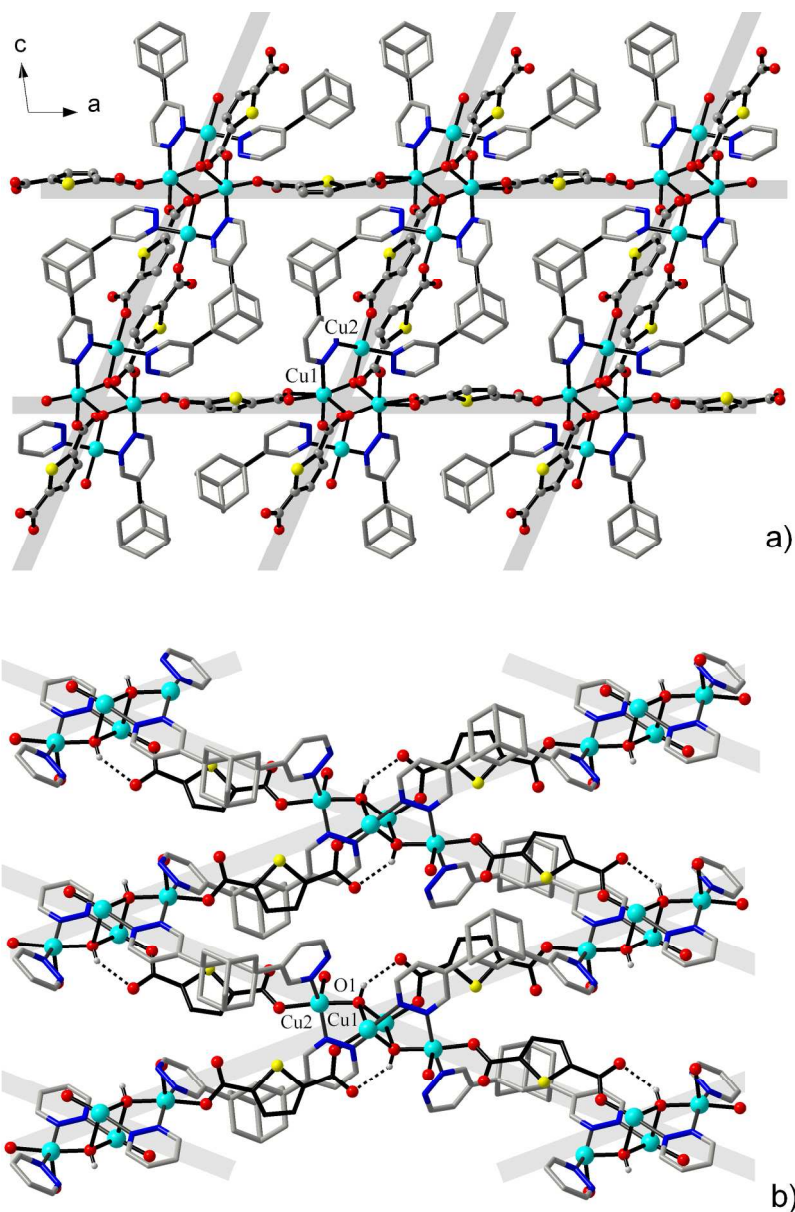
(a) Binuclear cluster in the environment of carboxylate and pyridazine ligands in the structure of 1; (b) 2D Cu/carboxylate subtopology in the form of hexagonal net, with the pyridazine-N donors accommodated at two sides of the plane. Only one orientation of the disordered cluster is shown.
230x375mm (300 x 300 DPI)



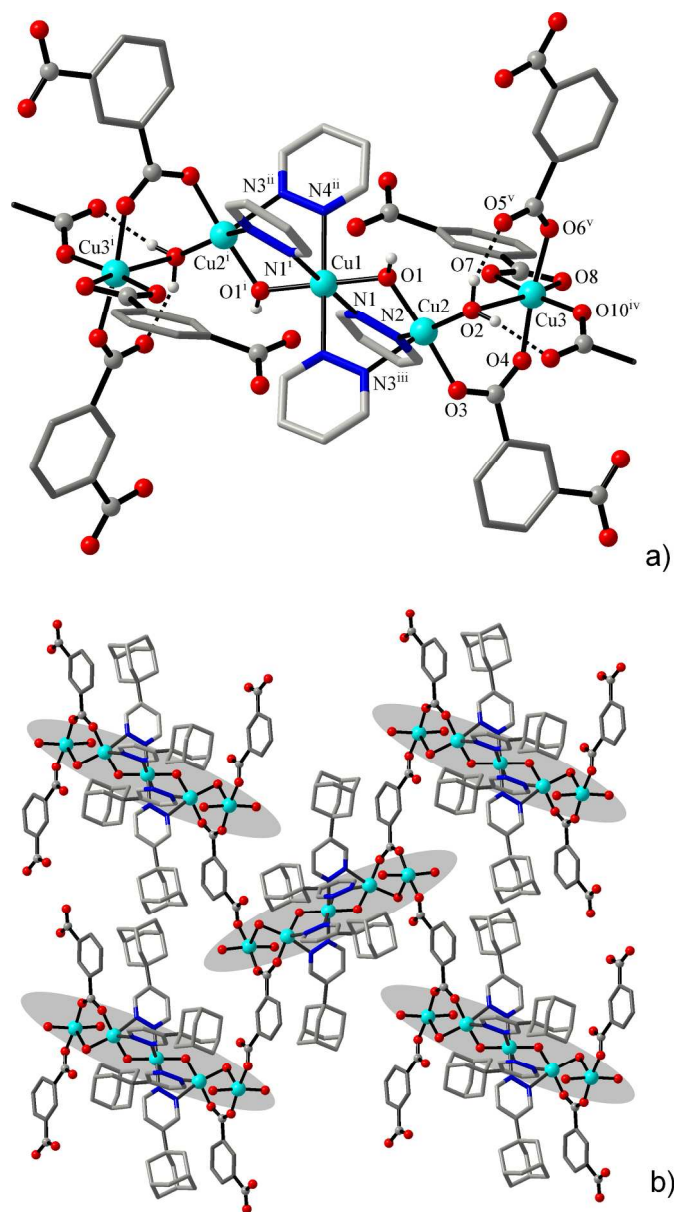
Interpenetration of two inversion-related 3D frameworks (marked with blue and grey bonds) in the structure of 1. The hydroxocopper-carboxylate layers are orthogonal to the drawing plane.
950x714mm (72 x 72 DPI)



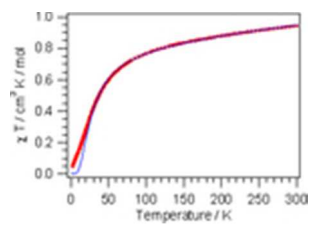
(a) Tetranuclear cluster in 2 showing the hydrogen bonding interactions with μ^3 -OH and aqua ligands; (b) Cu/carboxylate topology in the form of six- and three-connected CdI₂-like network. Note the intrinsic topological significance of the tricarboxylate linker. Symmetry codes: (i) $-x, 2-y, 1-z$; (ii) $-1+x, y, z$; (iii) $1-x, 1-y, 1-z$; (iv) $x, y, -1+z$.
240x444mm (300 x 300 DPI)



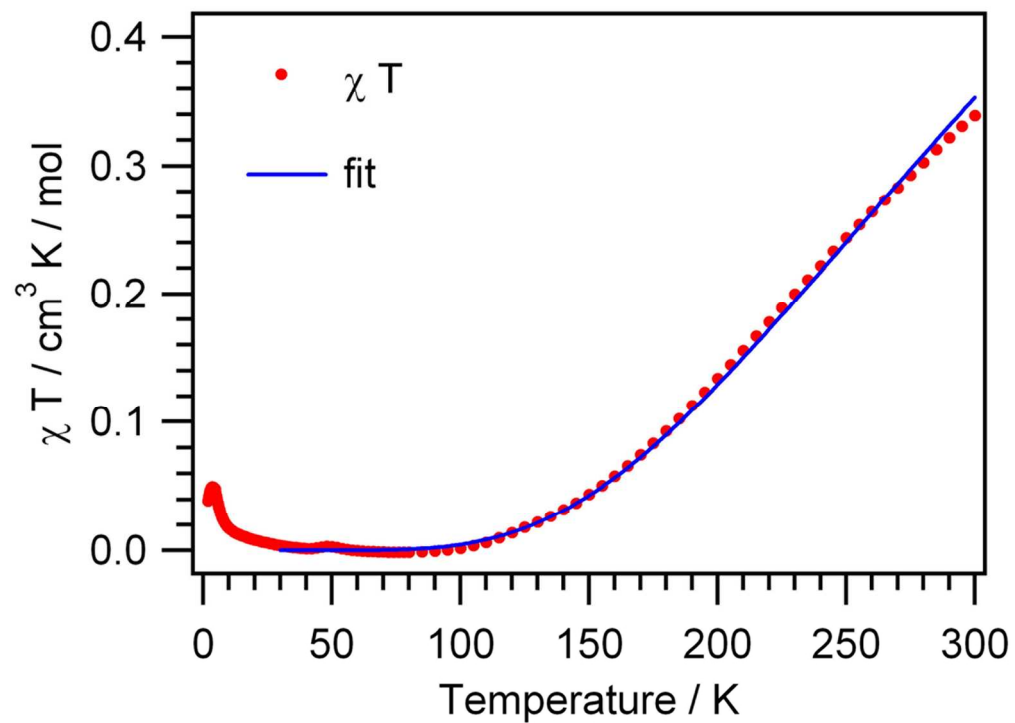
(a) Primitive cubic framework of 3 viewed down the b direction showing interconnection of heteroligand carboxylate/pyridazine planes by additional carboxylate linkers; (b) The heteroligand planes with double organic bridges between the tetranuclear clusters constituting the framework nodes.
210x317mm (300 x 300 DPI)



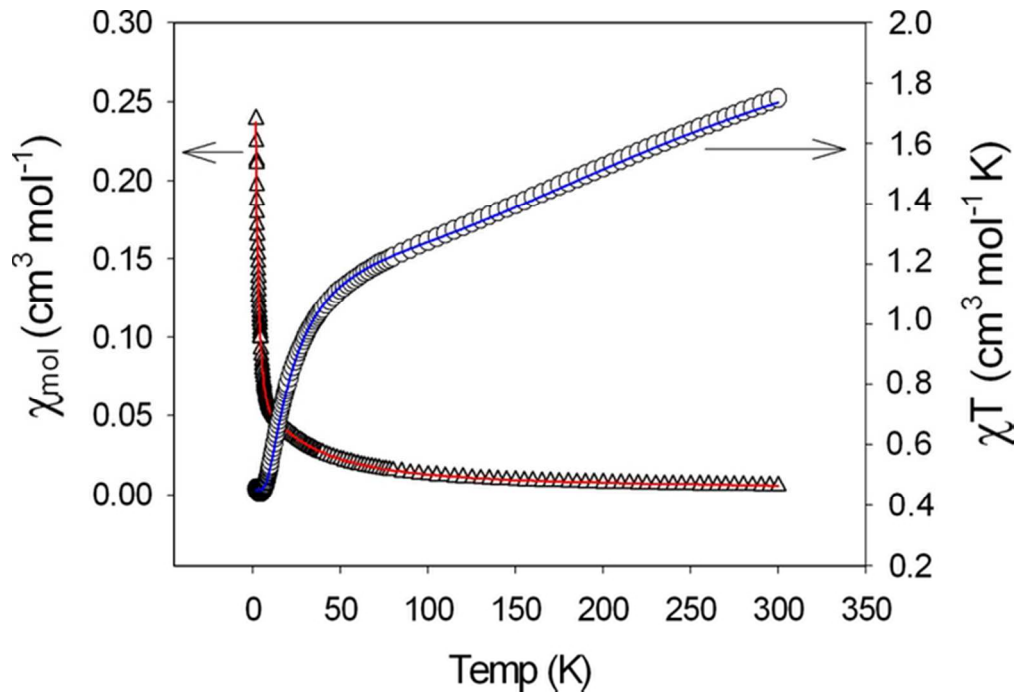
(a) Pentanuclear centrosymmetric clusters observed in 4 and 5. Note the compressed octahedral geometry around Cu1 ion. (b) Mode of interconnection of the clusters by dicarboxylate links. Symmetry codes: (i) $-x, -y, 2-z$; (ii) $0.5-x, 0.5+y, 2.5-z$; (iii) $-0.5+x, -0.5-y, -0.5+z$; (iv) $-1+x, y, z$; (v) $-0.5-x, 0.5+y, 2.5-z$.
224x407mm (300 x 300 DPI)



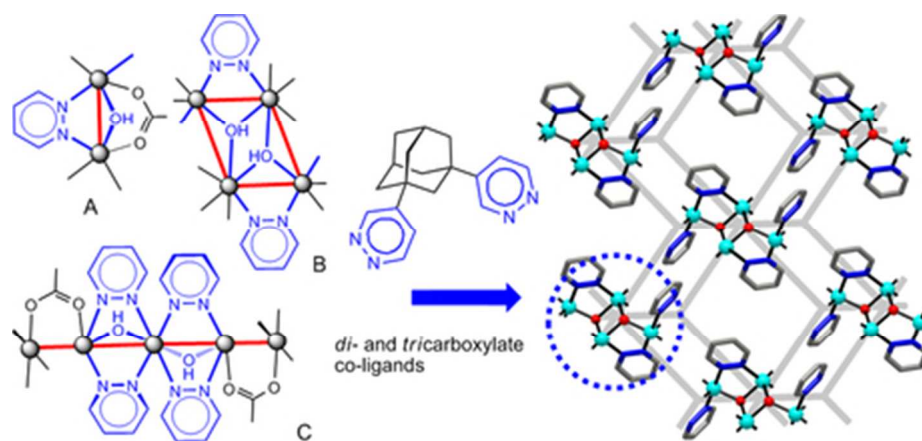
Thermal variation of χT for 1 (the solid line is drawn based on the Bleaney-Bowers equation).
12x8mm (300 x 300 DPI)



Thermal variation of χT for 3 (solid line is a fit according to equation 1).
105x77mm (300 x 300 DPI)



Thermal variation of χ_{m} and $\chi_{\text{m}}T$ for 4 (the solid lines are a fit to the data).
62x42mm (300 x 300 DPI)



Three types of polynuclear Cu(II) clusters rely on a compatibility of short-distance hydroxo-, carboxylato and pyridazine bridges and are applicable for the construction of 3D MOF structures incorporating complementary set of polyfunctional organic links.
38x18mm (300 x 300 DPI)